

Cosmology with Very-High-Energy Gamma Rays

To appear in ‘Advances in Very High Energy Astrophysics’, Mukherjee & Zanin, World Scientific (2022) <https://www.worldscientific.com/worldscibooks/10.1142/11141>

Elisa Pueschel¹ and Jonathan Biteau²

¹ Deutsches Elektronen-Synchrotron, D-15738 Zeuthen, Germany elisa.pueschel@desy.de

² Université Paris-Saclay, CNRS/IN2P3, IJCLab, 91405 Orsay, France biteau@in2p3.fr

arXiv:2112.05952v1 [astro-ph.HE] 11 Dec 2021

Introduction

Modern cosmology depicts the history of the universe as starting from a hot initial phase, filled with particles and antiparticles and expanding to eventually give rise to large-scale structures. While the first moments of the universe, near the Planck scale at $t_{\text{Pl}} = 5.4 \times 10^{-44}$ s, remain elusive on theoretical grounds, modern theories successfully describe the large-scale components and composition of the universe through a succession of epochs: inflation providing the flatness and causal connection of our universe; abrupt transitions describing the symmetry breaking of the electroweak and strong forces; decoupling of matter and radiation giving rise to the cosmic microwave background (CMB); the dark ages ending with the emergence of the first astrophysical sources of reionization; and finally the formation of structures and galaxies.

Observations constraining Big Bang Nucleosynthesis, the cosmic distance ladder, the spectrum and anisotropies of the CMB, and large-scale structures have been instrumental over the past fifty years in forming the modern vision of the universe’s history, yielding the current Λ CDM model largely dominated by cold dark matter (CDM) and dark energy (Λ). In this chapter, we discuss the contributions of gamma-ray astronomy at TeV energies to our understanding of the visible content and structure of the universe. We start from the present epoch with the second most intense electromagnetic background field after the CMB: the extragalactic background light (EBL). The EBL is composed of all the light emitted by stars and galaxies since the beginning of reionization, including light absorbed and re-emitted by dust. As such, the EBL traces the history of radiating matter in the universe. We then further dive into the large voids of the universe to study the large-scale magnetic fields that should permeate them. These fields could originate from the onset of structure formation or early phase transitions, bringing us back to the infancy of the universe. We conclude by looking back to the elusive Planck time scale, where the standard models of cosmology and particle physics are no longer applicable. Observations with current-generation gamma-ray astronomy experiments have now started to scratch the surface of cosmology, as we will show in this chapter.

7.1 The extragalactic background light

The study of the EBL is intertwined with an old scientific riddle, introduced by Digges in his English translation of Copernicus’ work (1576), further discussed by astronomers such as Kepler, Huygens, Halley, to be finally formulated in its mathematical version by de Chéseaux in 1744.

Let us divide a static, homogeneous and infinite universe in concentric shells of radius r and width dr . Each layer contains $4\pi r^2 dr \rho_*$ galaxies, with ρ_* their number density, and each galaxy emits a flux $L_*/4\pi r^2$, with L_* its individual luminosity. The flux reaching the observer from each shell is then a constant, $L_* \rho_* dr$, and the sum from multiple shells diverges when integrated over sufficiently great distances, resulting in an infinitely bright sky. This is known as the “dark night sky paradox” or Olbers’ paradox, from the amateur astronomer who popularized the riddle in the 19th century (Wesson, 1991). Both de Chéseaux and Olbers proposed an absorbing medium as a solution, but Herschel and Kelvin argued that absorption would inescapably lead to re-emission at longer wavelengths. The elucidation of the problem shook the premise of an infinite and immutable universe. Instead, light emission has a history which, from the epoch of reionization to the present epoch, is summarized in the starlight that composes the EBL.

7.1.1 Production and evolution: modelling the EBL

The EBL intensity and its shape as a function of wavelength are dictated by the cosmic star formation history (CSFH). Most of the direct and reprocessed emission from stars lies in the spectral range $0.1\ \mu\text{m}$ - $1000\ \mu\text{m}$: limited at its lower end by the Lyman limit ($0.0912\ \mu\text{m}$) and dominated at its higher end by the CMB. About half of the starlight emitted in the ultraviolet (UV, 0.1 - $0.3\ \mu\text{m}$), optical (0.3 - $0.8\ \mu\text{m}$) and near-infrared (NIR, 0.8 - $3\ \mu\text{m}$) bands escapes from galaxies, while the other half is absorbed by dust and reprocessed into the far-infrared band (FIR, 50 - $1000\ \mu\text{m}$). Accretion of matter onto supermassive black holes of active galactic nuclei (AGN) constitutes a secondary source of UV and optical photons, about half of which are absorbed and re-radiated in the mid-infrared band (MIR, 3 - $50\ \mu\text{m}$) by the hot dusty torii surrounding the accretion disks. Integrating the UV-FIR emission in time over the cosmic ages results in the broad-band EBL spectrum at $z = 0$ presented in Fig. 7.1. It features two broad components: the cosmic optical background (COB, 0.1 - $8\ \mu\text{m}$), composed of photons which escaped their environment without attenuation, and the cosmic infrared background (CIB, 8 - $1000\ \mu\text{m}$), composed of photons absorbed and re-radiated by dust. Because about half the light emitted by the sources of the EBL escapes directly from its environment and half is reprocessed, the bolometric intensities of the COB and of the CIB end up being comparable, both being compatible with $30\ \text{nW m}^{-2}\ \text{sr}^{-1}$, corresponding to a total energy budget for the EBL at the level of 6-7% that of the CMB. Three state-of-the-art models are compared in Fig. 7.1, each representing a distinct sub-class: empirical, phenomenological, and semi-analytic models.

Deep-field observations from UV-FIR satellites such as GALEX, Hubble, Spitzer, and Herschel have been key in deriving the luminosity functions of various galaxy types, down to sufficiently low luminosities that the integrated galaxy light converges at most wavelengths (Driver et al., 2016). These luminosity functions and associated observations are an important input to EBL models.

Empirical models (e.g. Domínguez et al., 2011, Franceschini and Rodighiero, 2017) exploit galaxy counts and inferred luminosity functions to cumulate average UV-to-FIR template spectra from various sub-types of galaxies. Phenomenological models (e.g. Andrews et al., 2018, Finke et al., 2010) additionally aim to reproduce the CSFH and evolution of metallicity. Combining constraints on the cosmic star-formation rate with the emission expected from each star, obtained e.g. from stellar population synthesis models for a given initial mass function, yields the direct emission contributing to the COB. The CIB is modelled assuming a fraction of reprocessed light and using template emission spectra for AGN and dust. These templates use high-quality spectral observations of galaxies, and include emission from amorphous or polycyclic aromatic hydrocarbons, resulting in the bump around $\sim 15\ \mu\text{m}$ visible in Fig. 7.1. Finally, semi-analytical models (e.g. Gilmore et al., 2012) additionally aim at tracking accretion throughout cosmic ages by exploiting N-body simulations of dark matter halo mergers. Such models can include baryonic physics, in particular AGN and supernova feedback, which affects the star-formation rate of their host galaxies.

All three types of models fundamentally aim at reproducing the emission from known, observed galaxies and as such reproduce in a fairly consistent manner the integrated galaxy light inferred from galaxy counts. This consistency is illustrated by a good match of the models around the peak of the COB at $1\ \mu\text{m}$. While some uncertainties remain in the UV range (see Khaire and Srianand, 2019 and references therein), the clearest mismatch between the models is observed at mid- and far-infrared wavelengths, where the amount of reprocessing by dust in the environment of the sources plays a key role. It should be noted that as current models aim at reproducing galaxy counts, they necessarily miss any unresolved population, such as primordial stars, and any truly

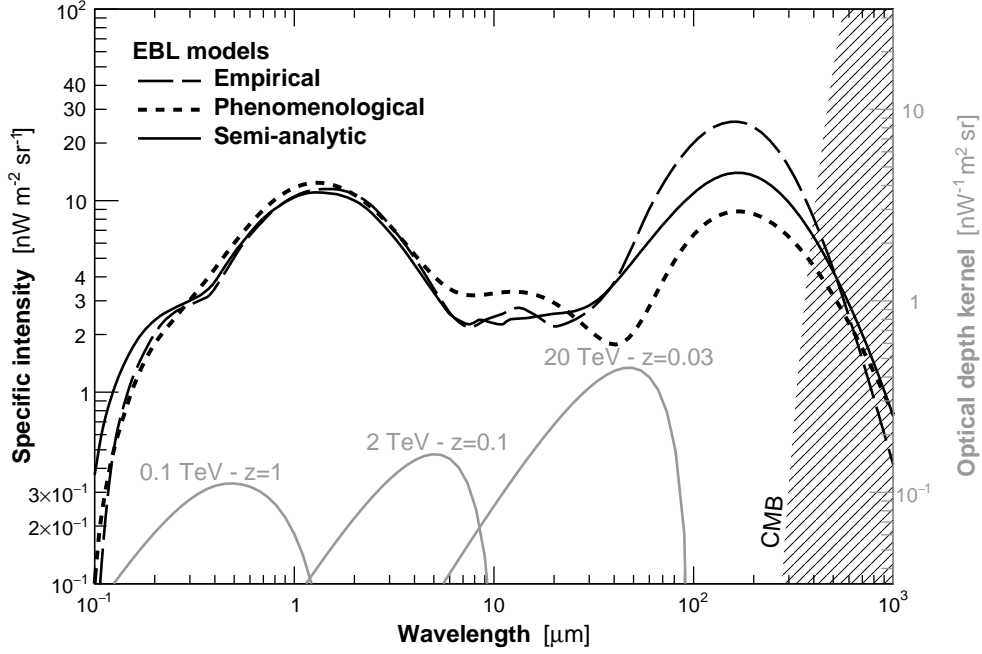


Figure 7.1: Spectrum of the EBL at $z = 0$, following the empirical model of [Domínguez et al. \(2011\)](#), the phenomenological model of [Finke et al. \(2010\)](#) and the semi-analytical model of [Gilmore et al. \(2012\)](#). The spectrum of the CMB, peaking around $1000 \text{ nW m}^{-2} \text{ sr}^{-1}$, is shown as a dashed area. Grey curves, denoted as “optical depth kernels” on the right-hand side axis, display the integral over redshift and angle of interaction of the pair production cross-section and evolution factors. The integral of the product of these functions and of the EBL intensity results in the gamma-ray optical depth, provided here at three characteristic energies and redshifts.

diffuse component.

7.1.2 VHE observables

The very-high-energy (VHE, $E_\gamma > 100 \text{ GeV}$) band opens a unique window on the density of EBL photons integrated over the line of sight, be they from known galaxies or of truly diffuse origin (see e.g. [Franceschini, 2021](#) for a recent review). Gamma rays from extragalactic sources can interact with EBL photons through the production of electron-positron pairs ([Gould and Schröder, 1967a,b](#), [Nikishov, 1962](#)). For this process to occur, the product of the gamma-ray energy, E'_γ , and of the EBL photon energy, ϵ' , as measured in the cosmological comoving frame, must satisfy a threshold condition imposed by kinematics, that is:

$$E'_\gamma \epsilon' \geq (m_e c^2)^2 \quad (7.1)$$

where $m_e c^2$ is the rest energy of the electron/positron.

The gamma-ray optical depth, $\tau(E_\gamma, z_0)$, with E_γ the gamma-ray energy in the observer’s frame and z_0 the redshift of the source, quantifies the number of interactions on the line of sight. As

indicated in Eq. (7.2), $\tau(E_\gamma, z_0)$ is the product of the EBL photon density, $\frac{\partial n}{\partial \epsilon}$ (units of $\text{cm}^{-3} \text{eV}^{-1}$), and of the differential cross section for pair production, $\sigma_{\gamma\gamma}$ (units of cm^2), integrated over the distance between the observer and the source, $\frac{\partial L}{\partial z}$ (units of cm), over the energy of the EBL photons, ϵ' (units of eV), and over the angle, θ , between the momenta of the gamma-ray and target EBL photons.

$$\tau(E_\gamma, z_0) = \int_0^{z_0} dz \frac{\partial L}{\partial z}(z) \int_0^\infty d\epsilon' \frac{\partial n}{\partial \epsilon'}(\epsilon', z) \int_1^{-1} d\cos\theta \frac{1 - \cos\theta}{2} \sigma_{\gamma\gamma}(E_\gamma \times (1+z), \epsilon, \cos\theta) \quad (7.2)$$

Using $\mu = \cos\theta$, the term $(1 - \mu)/2$ in the integral normalizes the cross section so that if it were isotropic ($\sigma_{\gamma\gamma}$ independent from θ), one would obtain $\int_{-1}^1 d\mu \frac{1-\mu}{2} \sigma_{\gamma\gamma} = \sigma_{\gamma\gamma}$.

The distance element in a flat Λ CDM cosmology, with H_0 the Hubble constant, Ω_Λ the dark-energy density, and Ω_M the matter-energy density, is given by:

$$\frac{\partial L}{\partial z} = \frac{c}{H_0} \frac{1}{1+z} \frac{1}{\sqrt{\Omega_\Lambda + \Omega_M(1+z)^3}}. \quad (7.3)$$

The Breit-Wheeler formula provides the pair creation cross section as:

$$\sigma_{\gamma\gamma}(\beta) = \frac{3\sigma_T}{16} (1 - \beta^2) \left[2\beta(\beta^2 - 2) + (3 - \beta^4) \ln\left(\frac{1 + \beta}{1 - \beta}\right) \right], \quad (7.4)$$

where σ_T is the Thomson cross-section, and β is given by:

$$\beta = \sqrt{1 - \frac{2(m_e c^2)^2}{E'_\gamma \epsilon'} \frac{1}{1 - \cos\theta}}, \quad (7.5)$$

The attentive reader should note that $E'_\gamma = E_\gamma \times (1+z)$ and ϵ' are the energies of the gamma-ray and EBL photon interacting at redshift z . It is worth noting that the physical condition that β be a real number and that $\sigma_{\gamma\gamma} \geq 0$ imposes the threshold condition:

$$E'_\gamma \epsilon' \geq \frac{2(m_e c^2)^2}{1 - \cos\theta}, \quad (7.6)$$

which translates to the lowest possible threshold for head-on collisions, i.e. Eq. (7.1) for $\theta = \pi$.

As illustrated in Fig. 7.1, the pair-production cross section, integrated over the line of sight,¹ has a full-width at half maximum covering almost a decade in EBL photon energy and peaking at an energy about twice that obtained from the threshold condition in Eq. (7.1). This results in gamma rays interacting preferentially with EBL photons in the wavelength range:

$$\lambda_{\text{EBL}} \simeq 0.5 - 5 \mu\text{m} \times \left(\frac{E_\gamma}{1 \text{ TeV}} \right) \times (1+z)^2 \quad (7.7)$$

where the factor $(1+z)^2$ accounts for the redshift of the energies of the photons. Interaction with photons from the CMB, which reaches an intensity comparable to that of the CIB around $\sim 250 \mu\text{m}$,

¹More accurately, we refer here to the quantity called ‘‘EBL kernel’’ (Biteau and Williams, 2015), properly normalized so that its unit is the inverse of that of the EBL intensity.

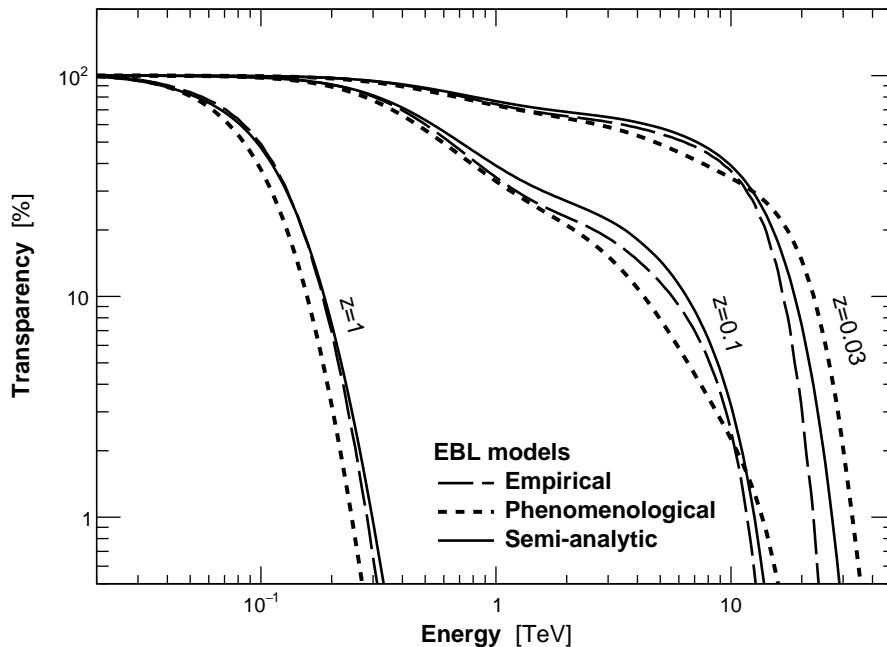


Figure 7.2: Attenuation factor, in percent, as a function of gamma-ray energy on Earth for sources located at $z = 0.03$, $z = 0.1$, and $z = 1.0$, following the empirical model of Domínguez et al. (2011), the phenomenological model of Finke et al. (2010), and the semi-analytical model of Gilmore et al. (2012).

becomes relevant for gamma-ray energies larger than ~ 50 TeV. From Eq. (7.7), one can infer that measurements of gamma-ray absorption around 20 TeV, obtained from nearby sources ($z \lesssim 0.05$), probe the CIB up to $100 \mu\text{m}$, while distant sources ($z \gtrsim 1$) detected up to a few hundred GeV probe the UV-optical part of the COB.

The transparency of the universe to gamma rays scales with the attenuation factor $\exp(-\tau(E_\gamma, z))$. At first order, the optical depth is a linear function of energy and of EBL photon density integrated over the line of sight, so that the transparency to gamma rays decreases with increasing energy and source distance, as illustrated in Fig. 7.2. Substructures can be identified in Fig. 7.2, with inflection points tracing the variations of the EBL spectrum as a function of wavelength. The features observed in the attenuation reflect the dependence of the EBL intensity on wavelength, with low-energy gamma rays (up to ~ 1 TeV) interacting with photons from the COB while higher-energy gamma rays interact mostly with photons from the CIB.

The gamma-ray spectrum observed from an extragalactic source is the product of the intrinsic spectrum of the source and of the attenuation factor, $\exp(-\tau(E_\gamma, z))$. The intrinsic spectrum is not *a priori* known, thus multiple features can be used to constrain or measure the EBL density: the variation of the spectral index from the unabsorbed region to the attenuated one (the $\Delta\Gamma$ method, e.g. Sanchez et al., 2013), the measurement of the cosmic gamma-ray horizon (the energy for which $\tau = 1$, e.g. Domínguez et al., 2013), and the reconstruction of the full spectral signature that is shown in Fig. 7.2 (Abramowski et al., 2013, Ackermann et al., 2012). The exploitation of these

features and the resulting constraints are further discussed in the next section.

7.1.3 VHE constraints

The extragalactic gamma-ray sky at GeV and TeV energies is dominated by blazars (BL Lac objects and flat-spectrum radio quasars), which have been detected by ground-based instruments to redshifts of about $z = 1$. The energy spectra of less distant sources can extend to high energies, in some cases to tens of TeV for sources with particularly hard intrinsic spectra (see [Biteau et al., 2020](#) for a review). Many blazars show dramatic flux variability. For example, up to ten thousand gamma rays have been collected in less than an hour during the highest states of the blazar PKS 2155-304 ([Aharonian et al., 2007](#)), enabling the construction of energy spectra with small statistical uncertainties. Blazars thus appear to be ideal gamma-ray beacons to probe the EBL. Long gamma-ray bursts (GRBs), a new class of VHE emitting sources, are also promising targets ([H. E. S. S. Collaboration et al., 2019, 2021](#), [MAGIC Collaboration et al., 2019b](#)). The current generation of imaging atmospheric Cherenkov telescopes (IACTs), together with *Fermi*-LAT ([Ackermann et al., 2012](#)), has mostly used blazar observations to probe the EBL spectral energy distribution (SED) (see e.g. [Desai et al., 2019](#)).

Individual measurements of sources at boundaries of the TeV-accessible redshift range ($z \sim 1$) are relevant for testing the redshift evolution of the EBL. Both MAGIC ([Ahnen et al., 2016](#), [Aleksić et al., 2015](#)) and VERITAS ([Abeysekara et al., 2015](#)) have detected flat-spectrum radio quasars at $z > 0.9$. Studies of the spectra of these sources have placed competitive constraints on the optical peak in the EBL SED. These measurements can be compared to EBL constraints obtained with nearby sources, which probe similar optical depths at the high-energy ends of their spectra. The comparison of measurements with low- and high-redshift gamma-ray sources provides an important consistency check for our understanding of the EBL evolution, provided that the EBL SED is well-constrained.

The most robust measurements use large ensembles of blazar spectra, mitigating the sensitivity to any unexpected spectral properties affecting individual sources. These include absorption of gamma rays by local radiation fields in the vicinity of the source ([Reimer, 2007](#)) and unaccounted-for variations in spectral shape over time.

While the latest EBL measurements have focused on a few well-tested methods, we pause briefly to describe alternative strategies. In one approach, intrinsic spectra in the VHE range were predicted from the blazars' multiwavelength SEDs (from radio to *Fermi*-LAT measurements), assuming that the SEDs could be described by synchrotron self-Compton models. The optical depth as a function of energy and cosmic gamma-ray horizon were calculated from the predicted and observed VHE spectra, and compared against EBL model predictions ([Domínguez et al., 2013](#)). The observed values were found to be consistent with model predictions.

Another method utilizes features in the optical depth as a function of energy. It is visible from [Fig. 7.2](#) that there is a flattening in the optical depth around 1 TeV (most visible for $z = 0.1$). This flattening should propagate to a significant change (a “break”) in spectral shape around 1 TeV for a precisely-measured energy spectrum. Testing for a spectral break in sources located at different redshifts thus provides an alternative method for probing the spectral shape of the EBL. Such a study was performed using *Fermi*-LAT and VHE spectra ([Orr et al., 2011](#)), and the authors estimated the EBL intensity at $15 \mu\text{m}$ to be $1.36 \pm 0.58 \text{ nW m}^{-2} \text{ sr}^{-1}$, while demonstrating agreement with model predictions at other wavelengths.

The study of [Abramowski et al. \(2013\)](#) established the first significant detection of the EBL

imprint at VHE and developed the basis of a method now commonly employed by the community. More recently, H.E.S.S. made a multi-source measurement of the EBL imprint using 21 spectra from nine blazars, covering a redshift range from $z = 0.031$ to $z = 0.287$ and an energy range from 190 GeV to 19.5 TeV (Abdalla et al., 2017). Datasets were divided into low- and high-flux states, resulting in multiple spectra per source for strongly variable sources, an approach, now standard, to address flux-level-dependent spectral variability. The method of measuring the EBL was to fit the spectra with a log-parabolic (or power law, in the case of no curvature) shape multiplied by an EBL attenuation factor of the form $\exp(-\tau(E_\gamma, z, \rho_i))$. Crucially, the level of the EBL intensity, denoted by the parameter ρ , was allowed to vary independently in several adjoining energy bands, indicated by the index i . This approach does not make any assumption about the shape or normalization of the EBL. The evolution of the EBL with redshift is tuned to replicate the predictions of Franceschini et al. (2008); this injects some dependence on a theoretical EBL model, although the impact is limited for gamma-ray sources with redshifts $z < 0.7$ (Biteau and Williams, 2015).

The combined best fit to all spectra reflects both the shape and normalization of the optical depth as a function of energy. The best fit including EBL attenuation was strongly favoured over a fit assuming no EBL attenuation, indicating evidence for a non-zero EBL at 9.5σ . The optical depth as a function of energy was translated back into an EBL intensity as a function of wavelength. The resulting EBL SED is shown in Fig. 7.3 (open squares labelled “B”). Both statistical and systematic uncertainties are shown. The latter are dominated by uncertainties on the H.E.S.S. energy scale.

Similar approaches to measuring the EBL were adopted by the MAGIC and VERITAS Collaborations (MAGIC Collaboration et al., 2019a, VERITAS Collaboration et al., 2019), using their own sets of blazar spectral measurements. In the case of MAGIC, contemporaneous *Fermi*-LAT spectra were also included, providing a more constraining fit, albeit with larger systematic uncertainties. VERITAS used a different analysis approach to that of MAGIC and H.E.S.S., testing the properties of a set of generic, smoothly varying EBL SED shapes. The results of both of these studies were consistent with the H.E.S.S. results.

A different, but also model-independent, approach was taken in a measurement of the EBL based on a large sample of archival spectral measurements (Biteau and Williams, 2015). Thirty sources and 86 spectra were analysed, bringing together spectral measurements from all of the current IACTs, as well as older instruments. Additionally, information from *Fermi*-LAT spectra was used, namely the requirement that the VHE spectra be softer than the contemporaneous *Fermi*-LAT spectra.

The EBL signature was detected at the 11σ confidence level, and the SED resolved as shown in Fig. 7.3 (filled squares labelled “A”). This strong detection and the relatively small errors on the points describing the EBL shape made it possible to disfavour several theoretical EBL models. The assessment of systematic uncertainties was, however, complicated by the use of archival measurements from multiple instruments. It should be noted that instrumental effects can be more thoroughly accounted for in the analysis of lower-level data.²

Selected results are summarised in Fig. 7.3. For clarity, Fig. 7.3 only shows the semi-analytic model of Gilmore et al. (2012). While no tension with the empirical model of Domínguez et al. (2011) was found in Biteau and Williams (2015), the phenomenological model of Finke et al. (2010) appears to be disfavoured due to an underestimation of the CIB amplitude, also suggested by the

²Besides the VHE energy scale, instrumental effects relevant to gamma-ray studies of the EBL in particular include energy resolution, and selection effects related to the choice of spectral points included in the analysis.

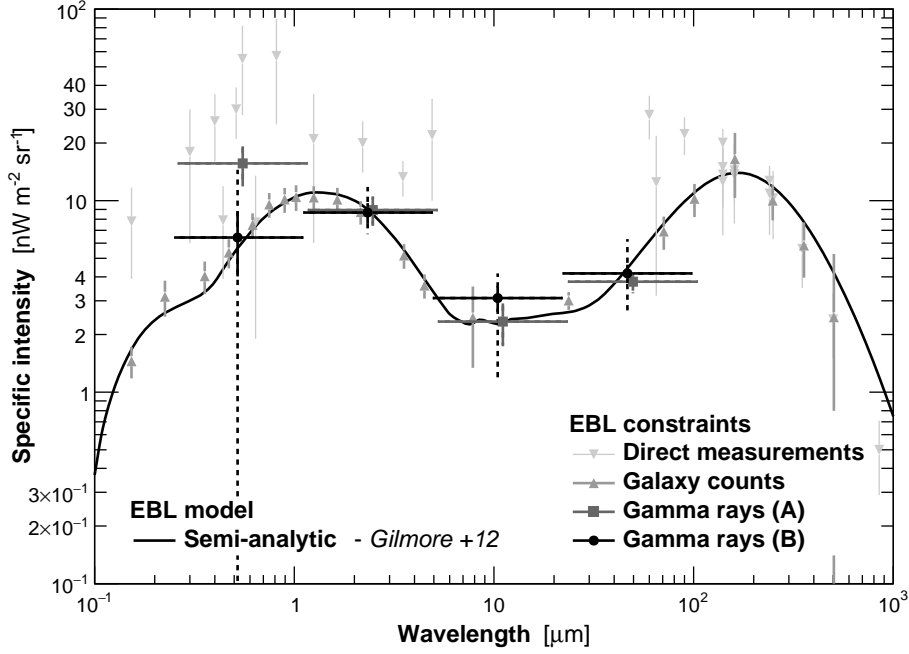


Figure 7.3: Observational constraints on the spectrum of the EBL at $z = 0$. Lower limits obtained from galaxy counts, which could miss unresolved populations or any truly diffuse EBL component, are shown as grey upward-pointing triangles (Driver et al., 2016). Constraints from direct measurements, possibly contaminated by foregrounds, are shown as light-grey downward-pointing triangles (Dwek and Krennrich, 2013). Gamma-ray measurements are taken from the works of Biteau and Williams (2015) (A) and Abdalla et al. (2017) (B). The semi-analytic model of Gilmore et al. (2012) is shown as a continuous line.

integrated galaxy light measured above $100 \mu\text{m}$ (Driver et al., 2016, Duivenvoorden et al., 2020). The most up-to-date empirical (Franceschini and Rodighiero, 2017, Saldana-Lopez et al., 2021) and phenomenological models (Andrews et al., 2018), driven by the recent gamma-ray detections and updated constraints from galaxy counts (Driver et al., 2016), show an agreement with the semi-analytic model of Gilmore et al. (2012) displayed in Fig. 7.3 at the 10 – 20 % level in the far-infrared region. This level of agreement suggests that both the models and the galaxy counts measurements are converging to comparable intensities not only in the wavelength region of the COB but also of the CIB.

We note that the current generation of IACTs has not reached the physical limit for resolving structures in the EBL spectrum, imposed by the natural width of the EBL kernel. Both of the measurements shown in Fig. 7.3 are based on large data samples, spanning years of observations and including bright flares. In spite of this, the EBL intensity can be extracted for only a limited range of EBL wavelengths, leaving ample room for progress with future observations.

7.1.4 Relation to non-VHE measurements

Our knowledge of the EBL benefits from the existence of a variety of measurement techniques beyond the VHE approach described above. Non-VHE measurements can be divided into direct measurements and constraints from galaxy counts (see [Driver, 2021](#), [Mattila and Väisänen, 2019](#) for reviews).

Direct measurements attempt to observe the sky (usually from space, as far from Earth as Pluto’s orbit for the New Horizons mission), and subtract off foreground contamination from non-EBL light (e.g. [Matsuura et al., 2017](#), [Zemcov et al., 2017](#)). This includes a number of light sources, some of which are diffuse/isotropic: stars, scattered light in Earth’s atmosphere, and light scattered by dust in the solar system (zodiacal light) and in the Milky Way. Due to the difficulty of adequately modelling and controlling against the foregrounds, direct measurements are generally treated as upper limits on the EBL intensity. Indeed, it has been pointed out that the spectrum of the EBL inferred from direct measurements shows similarities with the zodiacal light spectrum, suggesting an incomplete foreground subtraction ([Dwek et al., 2005](#)). An alternative approach that does not rely on the subtraction of a model-dependent foreground consists in measuring the night-sky brightness in the vicinity and within the shadow of a dark, opaque nebula. This approach has been used to measure the EBL intensity in the optical range and its results are consistent with integrated galaxy light and VHE measurements, albeit with larger uncertainties ([Mattila et al., 2017a,b](#)).

On the other hand, robust lower limits on the EBL intensity can be derived by summing the observed number of galaxies, accounting for their brightness, as a function of wavelength ([Driver et al., 2016](#), [Levenson and Wright, 2008](#), [Madau and Pozzetti, 2000](#)). These measurements have become increasingly precise as deep surveys have resolved fainter and fainter galaxies. One of the best examples to date lies in the $0.4 - 2 \mu\text{m}$ range, where a precision on integrated galaxy light close to 5% has been claimed ([Koushan et al., 2021](#)). However, such measurements are incapable of resolving diffuse emission. By comparing them to the VHE measurements, one can test for the presence of a diffuse component. It is interesting to note from [Fig. 7.3](#) that the EBL intensity derived from VHE measurements does not differ significantly from the integrated galaxy light. This rules out a large diffuse component of the EBL, although the uncertainties on both sets of measurements still allow for some diffuse contribution at the level of a few $\text{nW m}^{-2} \text{sr}^{-1}$.

The spectrum and evolution of the EBL are tightly connected with the history of star formation, including that of core collapse supernovae. The cumulative emission of neutrinos in the MeV energy range from all these objects builds up the diffuse supernova neutrino background ([Horiuchi et al., 2009](#)). A signal from the latter could start to emerge in future observations e.g. of the Super-Kamiokande Gadolinium experiment ([Lunardini, 2016](#)), providing constraints not only on the rate of core collapse supernovae but also on the CSFH and the initial mass function. The interplay of MeV neutrino measurements with high-precision EBL measurements provides exciting prospects for the understanding of the evolution of baryonic matter in the universe.

Finally, gamma-ray constraints on the EBL, particularly in the FIR band, could help further constrain the propagation of other astrophysical particles: ultra-high-energy cosmic rays (UHECR), which are nuclei with energies larger than 10^{18} eV ($\equiv 1$ EeV). UHE protons interact with CMB photons through the so-called Greisen-Zatsepin-Kuzmin (GZK) effect, losing energy via pion and electron-positron pair production. Heavier nuclei, ranging from He to Fe, can also photodissociate on low-energy photon fields, i.e. release a neutron or a proton carrying a fraction of the energy of the parent nucleus. Photodissociation on FIR EBL photons is the dominant energy-loss process

for low-to-intermediate mass nuclei with a Lorentz factor $\Gamma \sim 10^9$ (Alves Batista et al., 2015). The uncertainty on the intensity of the CIB, as shown in Fig. 7.1, has a non-negligible impact on the interpretation of the UHECR spectrum above a few tens of EeV. It additionally impacts the flux of cosmogenic neutrinos, i.e. those produced along the line of sight by UHECR, particularly around 10^{17} EeV.

7.1.5 Connecting the EBL and the Hubble constant

An enticing inversion of EBL measurements is to use the same VHE gamma-ray propagation effects to measure the Hubble constant, H_0 . Proposed from the early days of gamma-ray astronomy (Barrau et al., 2008, Blanch and Martinez, 2005a,b,c, Salamon et al., 1994), this alternative method of measuring H_0 remains relevant, as tension between different measurements of H_0 persists at a significance currently estimated to be larger than 4σ (Di Valentino et al., 2021). Two approaches have been employed to constrain the universe’s expansion rate with measurements of gamma-ray absorption.

The first approach, largely independent of the EBL model, consists in comparing the integrated galaxy light to the gamma-ray optical depth inferred from VHE emitters in the local universe ($z \leq 0.2$), where evolutionary effects have a negligible impact on gamma-ray absorption. Such approaches are labeled here as “gamma-ray/local EBL”. Since the optical depth is the product of the EBL intensity, pair-production cross-section and distance element, with the latter scaling as H_0^{-1} , the Hubble constant can be constrained by assuming that the EBL consists entirely of integrated galaxy light. The latter measurements are independent of the Hubble constant, but may underestimate the total EBL, particularly if truly diffuse components or unresolved populations of UV-optical photons are non-negligible.

The second approach exploits the latest models of the EBL which aim at reproducing the galaxy counts that result in the integrated galaxy light, in addition to the CSFH and metallicity evolution for phenomenological models. Such approaches are labeled here as “gamma-ray/CSFH”. For a fixed astrophysical model, the additional dependence of the EBL density on the Hubble constant, scaling as H_0^3 , provides a further handle on the universe’s expansion rate. This approach is more sensitive to variations of the Hubble constant but could also be more dependent on the underlying astrophysical model.

The first measurements exploiting the local (Biteau and Williams, 2015) and evolutionary techniques (Domínguez and Prada, 2013) were dominated by systematic uncertainties on the integrated galaxy light and EBL model, respectively, as well as those on the gamma-ray energy scale. As shown in Fig. 7.4, the systematic uncertainties on H_0 are on the order of $10 - 15 \text{ km s}^{-1} \text{ Mpc}^{-1}$, preventing a useful contribution to the debate between early-type and late-type measurements of H_0 , which differ by about $5 \text{ km s}^{-1} \text{ Mpc}^{-1}$. Recently, Domínguez et al. (2019) further developed the evolutionary approach and tested both the phenomenological model of Finke et al. (2010) and the empirical one of Domínguez et al. (2011) against the cosmic gamma-ray horizon inferred from VHE archival data and *Fermi*-LAT data. The authors claimed a measurement with an accuracy of $3 \text{ km s}^{-1} \text{ Mpc}^{-1}$ when fixing Ω_M to its reference value and with an accuracy of $6 \text{ km s}^{-1} \text{ Mpc}^{-1}$ when leaving Ω_M free (the former is reported in Fig. 7.4).

Independent analyses are critically needed to assess and compare the potential of such gamma-ray constraints. If confirmed, current and future gamma-ray observations could provide relevant inputs to the debate on the current cosmological paradigm. The number of extragalactic gamma-ray sources detectable by the Cherenkov Telescope Array (CTA) and the ability to measure their

redshifts will be key in the development of this scientific avenue.

7.1.6 Outlook

The EBL encodes information about the CSFH and accretion of matter over cosmic ages. Ground-based gamma-ray astronomy is now mature enough to detect the imprint of the EBL in the spectra of gamma-ray blazars and measure the EBL spectrum at $z = 0$ from optical to MIR wavelengths.

Nonetheless, wide areas of research on the EBL remain open. Tighter constraints on the UV part of the EBL spectrum, probed by distant sources beyond $z = 1$, will provide insight into the role of the AGN in ionizing the universe (Andrews et al., 2018). The signature of polycyclic aromatic and amorphous hydrocarbons, responsible for the bump around $15 \mu\text{m}$ in the models shown in Fig. 7.1, remains undetected at multi-TeV energies. Theoretical and observational uncertainties in the FIR band, which could be solved by high-quality measurements beyond 10 TeV, still hinder a full grasp of UHECR propagation. Exciting prospects can also be found in the detection of the spectral signature of the first stars, microquasars or outflows that may have been responsible for the reionization of the universe. The signature is expected to be visible as a broad feature above $1 \mu\text{m}$, in the core EBL wavelength range probed by TeV instruments (Gilmore, 2012). Finally, the wavelength range close to the peak of the COB offers interesting prospects for constraining the amount of light emitted at the outskirts or even outside of galaxies, by stars in the intra-halo, intra-group and intra-cluster media (Mattila and Väisänen, 2019).

Besides providing a wide wavelength coverage of the EBL thanks to its order of magnitude improvement in sensitivity with respect to current-generation instruments, CTA will also enable the study of the evolution of the EBL, by reconstructing the absorption in successive layers of redshift (CTA Consortium et al., 2021). The expected accuracy on the EBL reconstruction is two-to-three times better for CTA than for current-generation instruments, and it is anticipated

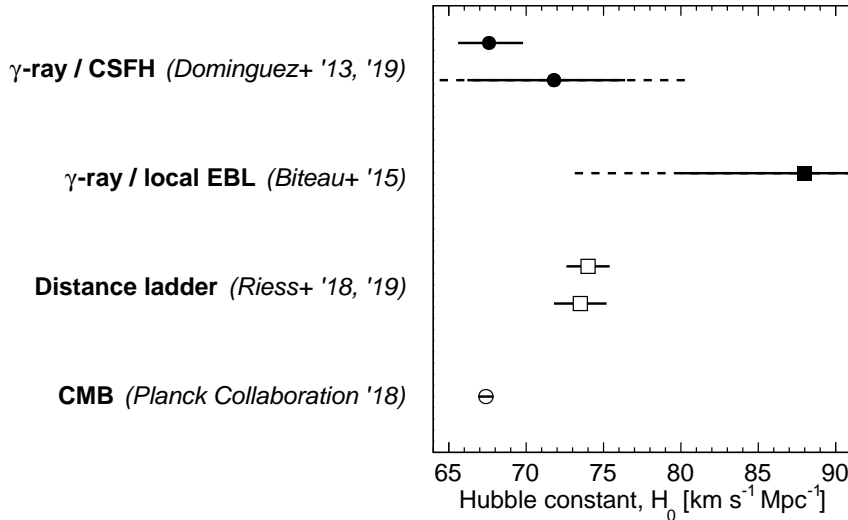


Figure 7.4: Comparison of measurements of the Hubble constant by Planck (Ade et al., 2016a) and the Hubble Space Telescope (Riess et al., 2018) with VHE gamma-ray measurements (Biteau and Williams, 2015, Domínguez and Prada, 2013, Domínguez et al., 2019).

that EBL constraints will be derived with gamma-ray sources located at redshifts as distant as $z = 2$. This will enable ground-based gamma-ray astronomy to place meaningful constraints on the CSFH, as recently done by [Fermi-LAT Collaboration et al. \(2018a\)](#). The low-energy threshold of CTA will further help in disentangling intrinsic spectral curvature due to internal absorption processes, energy cut-offs related to particle acceleration and escape, and extrinsic spectral features due to the propagation of gamma rays on cosmological scales. Finally, it is expected that CTA will set robust constraints on the Hubble constant, testing the current cosmological paradigm.

7.2 The intergalactic magnetic field

Understanding the generation and evolution of large-scale magnetic fields in the universe is a key topic in cosmology, and one for which persistent questions remain. Magnetic fields permeate the universe from scales as small as stars, to galaxies and galaxy clusters, to the filaments separating the voids in the large-scale structure, and at the largest scales, to the voids themselves.

Two possibilities have been proposed for the origin of cosmological magnetic fields: primordial and astrophysical origin. In the former case, a weak magnetic field is generated in phase transitions in the early universe. This “seed” field is then amplified in astrophysical systems to the strong magnetic fields ($\sim \mu\text{G}$ or greater) observed in galaxies and galaxy clusters. In the latter case, the magnetic fields are generated and amplified within galaxies and then ejected beyond the immediate environment of the astrophysical accelerator into the intergalactic medium. The timing of the magnetic-field generation is notably different in the two cases: shortly after the Big Bang, or after the onset of galaxy formation. This difference propagates to differences in the magnetic-field strength, correlation length (distance over which the field behaves coherently), and the evolution of the magnetic energy density with redshift in the different generation scenarios.

It is worth briefly discussing the underlying mechanisms for the generation and amplification of magnetic fields in plasmas. A magnetic field in a plasma can be spontaneously generated via the Biermann battery process. In a plasma with a temperature and density gradient, the lighter free electrons drift down the pressure gradient faster than protons. For misaligned temperature and density gradients, this creates an electromotive force that generates a magnetic field. Once created, a weak magnetic field can be amplified via dynamo mechanics. The movement and rotation of plasma in an astrophysical system stretches and compresses magnetic-field lines, amplifying the field as kinetic energy is converted into magnetic energy.

Extracting clues about magnetic-field generation from observations of magnetic fields in galaxies and filaments is extremely difficult due to the uncertainties associated with the dynamics of the amplification process. On the other hand, the magnetic field in the voids of the large-scale structure—the intergalactic magnetic field (IGMF)—reflects the conditions of its generation for primordial production scenarios. In the case that the magnetic fields in the voids are not primordial, but due to plasma outflows from astrophysical systems, they would provide information about the efficiency of magnetic energy transfer into the voids. Consequently, regardless of the generation scenario, magnetic fields in voids are of particular interest ([Durrer and Neronov, 2013](#), [Neronov and Semikoz, 2009](#)).

Measuring the IGMF poses experimental challenges, primarily because it is expected to be extremely weak. While some experimental and theoretical bounds exist, the allowed range of strength and correlation length is distressingly broad, as shown in [Fig. 7.5](#) ([Alves Batista and Saveliev, 2021](#)). The lowest guaranteed theoretical bound on the IGMF exploits the Harrison effect

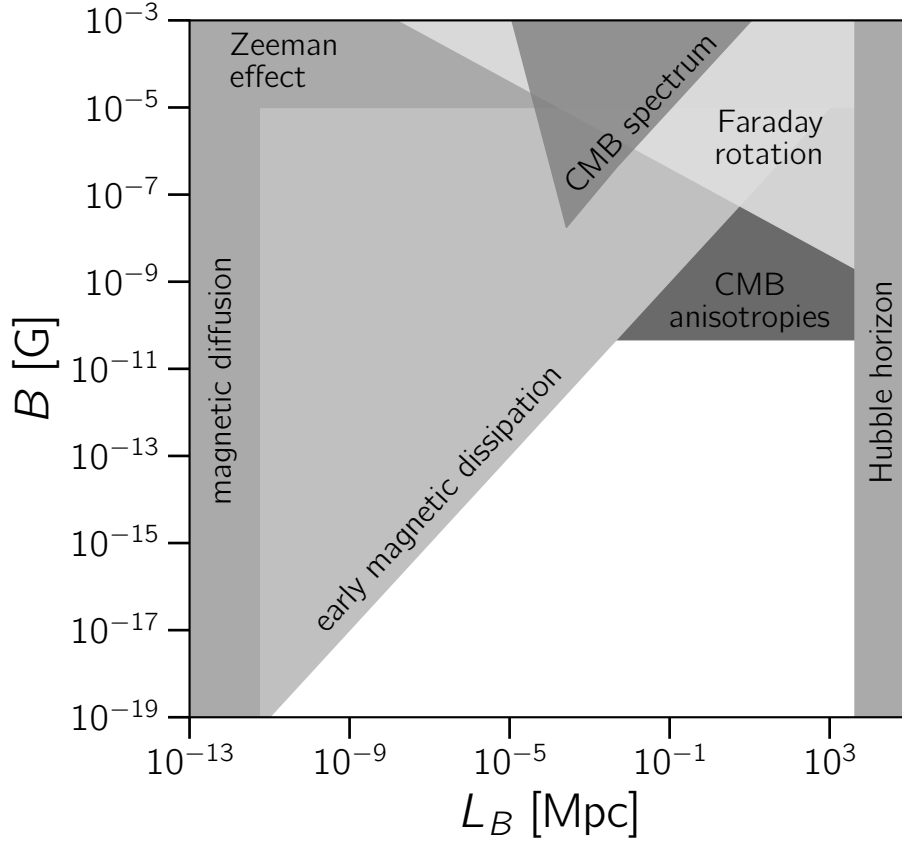


Figure 7.5: The allowed region of IGMF strength and correlation length. Bounds from non-VHE measurements (discussed in the text) are shown by the shaded regions. Credit: Rafael Alves Batista, adapted from [Alves Batista and Saveliev \(2021\)](#).

([Harrison, 1970](#)). Magnetic fields are generated during the radiation-dominated era due to the difference in angular momentum of electron-photon and ion gases as rotating protogalaxies expand. The minimum magnetic field strength generated by this process gives a lower bound on the IGMF strength in voids of 10^{-29} G for a correlation length of 10 Mpc. The gamma-ray measurements described below set more aggressive lower limits on the IGMF strength.

7.2.1 Field generation

Early universe

Magnetic fields can be generated in the early universe due the charge separation that occurs during phase transitions. The Hubble horizon at the time of field generation determines the possible range of correlation lengths for the case of magnetic fields generated after inflation. An IGMF generated during a QCD phase transition, for example, is expected to have a longer correlation length than one generated during an electroweak phase transition, although it must be noted that there is a large overlap region in the strength and correlation length predictions in the two generation scenarios (see e.g. [Neronov and Semikoz, 2009](#)). The correlation length of inflation-generated magnetic

fields, on the other hand, is not limited by the Hubble horizon, and can reach the current horizon scale (Kahniashvili et al., 2016).

Astrophysical

Turbulent plasma movement occurs in a number of astrophysical systems and could lead to the injection of magnetic fields into the intergalactic medium. Star formation activity and supernovae in starburst galaxies are candidates for IGMF generation. Starburst activity of early-forming dwarf galaxies at a time when the universe was smaller and more densely packed could also plausibly magnetise the intergalactic medium. Alternatively, at later stages in the universe’s evolution, the giant lobes of radio galaxies and the jets of active galactic nuclei could expel magnetised plasma; indeed, much more energy is available from these sources than from the outflows of starburst galaxies.

The expected correlation length for an astrophysically generated IGMF is shorter than for a primordial field, due to the later generation. The field strength is expected to be high in the vicinity of the generating sources, but to decay steeply toward zero in voids. The predicted strength in the voids is of order 10^{-10} G or less, several orders of magnitude less than the strength in sheets and filaments (Neronov and Semikoz, 2009, Vazza et al., 2017).

Beyond strength and length

In addition to measuring the strength and correlation length of the IGMF, constraining its helicity is of particular interest, both for understanding the conditions at generation, and for modelling its evolution (Vachaspati, 2021). The diffusion of magnetic energy from small scales to large scales depends on the helicity of the field, with a slower dissipation time for helical fields (Neronov and Semikoz, 2009).

Lastly, measuring the redshift evolution of the field strength and energy density is important for tracing the generation of the field. An astrophysically generated IGMF is expected to have a lower energy density at high redshifts than in the local universe.

7.2.2 VHE observables

We have already discussed the impact of the EBL on VHE photons travelling from distant blazars. Neglected in that discussion was the further trajectory of the electron-positron pairs produced in interactions with EBL photons. As charged particles, they are deflected by the IGMF, prior to interacting with the CMB. The electrons and positrons upscatter the CMB photons to higher energies via inverse Compton scattering. For sufficiently high energy particles, the process repeats and an electromagnetic cascade develops. A useful estimation of the energies involved is given in Neronov and Semikoz (2009):

$$E_\gamma = \frac{4}{3}(1 + z_{\gamma\gamma})^{-1} \epsilon_{\text{cmb}} \frac{E_e^2}{m_e^2 c^4} \simeq 0.32 \text{ TeV} \left[\frac{E_{\gamma_0}}{20 \text{ TeV}} \right]^2 \quad (7.8)$$

for which E_γ is the energy of the observed photon on Earth, E_{γ_0} is the energy of the primary photon at the source, m_e and E_e are the mass and energy at pair production of the electron or positron, and $\epsilon_{\text{cmb}} = 0.6 \text{ meV}(1 + z_{\gamma\gamma})$ is the CMB photon energy. A ~ 10 TeV primary photon is thus reprocessed to ~ 100 GeV, not far above the energy threshold of current-generation IACTs.

Deflection of the electrons and positrons by the IGMF broadens the cascade in space and delays the cascade arrival time at the observer by increasing the path length from the pair-production site to the observer. Both of these effects make it possible to probe the IGMF strength along the line of sight with observations of the VHE gamma-ray emission of distant blazars.

The narrowly beamed ensemble of relativistic electron/positron pairs constitutes a plasma, and can develop electromagnetic and electrostatic plasma beam instabilities. Whether these instabilities develop faster than the timescale for inverse Compton scattering, and how efficiently they dissipate energy into the intergalactic medium, is important for understanding whether inverse Compton scattering is the dominant cooling process and whether an electromagnetic cascade can indeed develop (Broderick et al., 2012). Some simulations indicate that beam cooling from plasma instabilities is not expected to be a large effect in the case of cascades from TeV blazars (Rafighi et al., 2017, Sironi and Giannios, 2014). However, other results indicate that the beam cooling from plasma instabilities could proceed on a similar timescale to inverse Compton cooling, reducing the expected cascade emission (Vafin et al., 2018). The theoretical debate on this topic thus awaits conclusive answers. The reader should note that the results that follow assume that inverse Compton scattering is the dominant cooling process.

Spectral signature

Due to the reprocessing of emission from higher to lower energy, the shape of the GeV-TeV spectrum is sensitive to the IGMF strength. Some fraction of electron/positron pairs are deflected out of the observer’s field of view for a non-zero IGMF, reducing the number of observed GeV gamma rays and the relative ratio of GeV to TeV emission. By comparing the observed source spectrum with predicted spectra with and without considering an IGMF, it is possible to set lower limits on the IGMF strength. However, it is necessary to make some assumptions about the shape of the intrinsic source spectrum.

Blazar flux variability is an important confounding factor in such studies. Unless the GeV and TeV observations are made simultaneously, it is impossible to differentiate an IGMF-induced effect from sampling different flux states with the GeV and TeV observations.

Pair halos and magnetically broadened cascades

A second approach for measuring the IGMF is to search for a low-energy angular extension produced by angular broadening of the cascade emission. As distant sources, even the closest blazars are expected to be point-like within the angular resolution of the current instruments. However, depending on the strength of the IGMF, two types of angular extension can occur, referred to here as pair halo and magnetically broadened cascade. The key point is that some fraction of electrons (positrons) isotropize in the magnetic field and gyrate around their point of production. The stronger the IGMF, the higher the energy of the charged particles that are isotropized.

A pair halo refers to the case where a strong IGMF (10^{-12} – 10^{-9} G) isotropizes a large fraction of high-energy charged particles in the cascade, causing them to accumulate around the source. The reprocessed emission arriving at the observer is consequently extremely time-delayed, on the order of hundreds of years (Eungwanichayapant and Aharonian, 2009).

In the case of magnetically broadened cascades, a weaker IGMF (10^{-16} – 10^{-12} G, still strong enough to produce an extension beyond the point spread function of current instruments) isotropizes only lower energy charged particles, while much of the cascade travels to the observer with time

delays of the order of years with respect to the primary emission.

Predictions for angular extensions can be arrived at through analytic approximations (Dermer et al., 2011, Neronov and Semikoz, 2009). An approximation of the deflection angle of an inverse Compton gamma ray illustrates the important factors (Neronov and Semikoz, 2007):

$$\theta_{ext} \simeq \frac{0.7^\circ}{\tau(E_{\gamma_0}, z)} \left[\frac{E_\gamma}{6 \text{ TeV}} \right]^{-1} \frac{B}{10^{-13} \text{ G}}. \quad (7.9)$$

As expected, the extension scales with the IGMF strength B , and inversely with the energy of the upscattered photon E_γ . It also depends on the optical depth for the primary photon (the equation holds for $\tau > 1$). Consequently, the more distant the source and higher the energy of the primary photon, the smaller the predicted extension. This only holds to a point: if the mean free path of the primary gamma ray has the same scale as the distance to the observer, the cascade will not have developed enough to be observable by the time it reaches the observer. Consequently, sources at $z \simeq 0.1\text{--}0.2$ are particularly suitable for IGMF studies in the energy range of interest for IACTs.

7.2.3 Simulating cascades

In addition to analytical approximations, there are an abundance of numerical simulations, which treat the cascade process and magnetic-field structure with varying levels of detail (Abramowski et al., 2014, Alves Batista et al., 2016, Archambault, S. and others, 2017, Arlen et al., 2014, Eungwanichayapant and Aharonian, 2009, Finke et al., 2015, Fitoussi et al., 2017, Kachelriess et al., 2012, Taylor et al., 2011). Numerical simulations, although often computationally intensive, provide more accurate predictions of the cascade spectrum and angular extension, and the ratio of cascade to total emission (cascade fraction). They also allow a detailed treatment of the primary spectrum of the source, most commonly taken as a power law with an exponential cutoff at high energy in the literature. The impact on the cascade emission of factors such as the Doppler factor of the blazar jet, the viewing angle of observer with respect to the jet, and the choice of EBL model can also be studied.

7.2.4 VHE constraints

Similarly to EBL studies, hard-spectrum blazars, particularly extreme TeV blazars, are good candidates for IGMF studies (Biteau et al., 2020). As discussed previously, the primary emission is reprocessed to much lower energies through the cascade development. The cascade emission coming from sources with soft spectral indices and low-energy (sub-TeV) spectral cutoffs falls below the GeV-TeV energy range. Extreme blazars thus represent the most viable candidates for setting VHE constraints on the IGMF.

The constraints presented below can be best read as order-of-magnitude estimates. The uncertainties on predictions of the cascade emission are still large and have a strong impact on the derived constraints.

Constraints from spectral measurements

Many attempts have been made to set lower limits on the IGMF strength based on the GeV-TeV broadband spectrum. We only discuss selected results here. All studies nominally assumed a correlation length $\lambda_B \geq 1 \text{ Mpc}$.

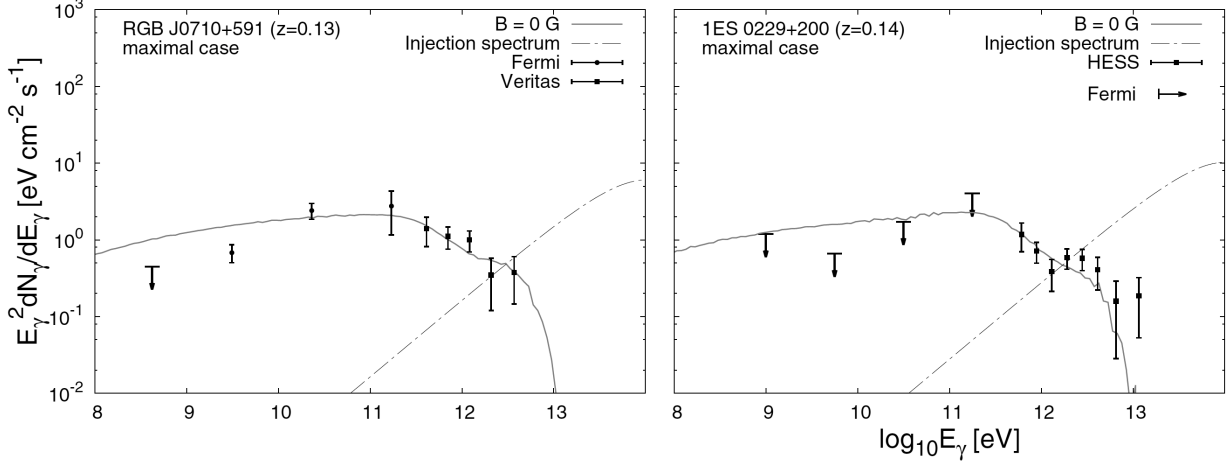


Figure 7.6: The *Fermi*-LAT/VHE spectra for two gamma-ray blazars, shown with the predicted cascade component in the absence of IGMF (solid line). The predicted GeV component of the spectrum is higher than the observed flux. The upper bounds denoted by the arrows show the 99% confidence level. The dashed line denotes the injection spectrum, prior to the cascade development. Figure extracted from Taylor et al. (2011).

An early study used archival TeV spectra of three hard-spectrum blazars together with simultaneous *Fermi*-LAT observations to produce broadband spectra (Taylor et al., 2011). These were then fit with numerical predictions for the spectral shape with and without IGMF. Example spectra are shown for illustration in Fig. 7.6. As shown in the figure, the predicted spectrum for IGMF strength $B = 0$ overshoots the observed *Fermi*-LAT flux. Assuming the GeV deficit is due to the cascade emission being deflected out of field of view of the observer, B must be at least $\sim 10^{-15}$ G. Taking the pessimistic assumption that the source was only active during the observation time (three years at the time the study was made) and the GeV deficit is due to the time delay of the cascade emission with respect to the primary emission, a lower limit of $B \gtrsim 10^{-17}$ G was obtained.

A later study used the four blazar datasets of Taylor et al. (2011) as well as four additional hard-spectrum blazars (Arlen et al., 2014). Here, a scan was made of the possible parameters (jet opening angle, Doppler factor, etc.) within reasonable limits. Accounting for these uncertainties, the authors concluded that the broadband spectra are compatible with $B = 0$. Some tension was observed in the case of one source (1ES 0229+200), however it was noted that this could be resolved by shifting the assumed EBL shape within experimental uncertainties.

An overlapping set of sources, covering observations of five hard-spectrum blazars, and including several more years of *Fermi*-LAT data than previous studies, has also been considered (Finke et al., 2015). While an analytical approach to the cascade predictions was taken, the predicted cascade spectra were checked against simulation. An IGMF strength less than 10^{-19} G was ruled out at $\geq 5\sigma$ confidence.

Constraints from searches for angular extension

All of the currently operating IACT collaborations have made searches for angular emission around blazars. Searches for extended emission have the advantage that they can be carried out by a

single instrument. The sensitivity to extended cascade emission is driven by two factors: the energy threshold and the angular resolution of current-generation IACTs. The former determines the total measurable flux of cascade emission, the latter is directly correlated to the smallest detectable extension and the weakest detectable IGMF. A standard approach has been to compare the angular profile observed in data to the prediction for a simulated point source, where the extension is entirely due to the instrument point spread function.

An early attempt was made by MAGIC to constrain the IGMF with a search for extended emission around the nearby blazars Markarian 501 and Markarian 421 (Aleksić et al., 2010). In lieu of the detection of an IGMF signature, placing constraints is complicated by the close proximity of the sources, their extreme variability, and the presence of source-intrinsic spectral cutoffs.

H.E.S.S. studied three hard-spectrum blazars located at redshifts $z = 0.140 - 0.186$, using numerical simulations to predict the cascade flux and angular profile (Abramowski et al., 2014). An example of the angular profile in data and simulation is shown in Fig. 7.7. Extended emission was ruled out at the level of a few percent of the Crab nebula flux for the most constraining source. Additionally, H.E.S.S. set limits on the cascade fraction, which were translated into a limit on the IGMF strength. The cascade simulation predicts the cascade fraction and angular extension as a function of IGMF strength for an assumed intrinsic spectrum. Fig. 7.7 shows the evolution of the predicted cascade fraction as a function of IGMF strength, compared to upper limits on the cascade fraction extracted from data. The latter are produced by finding the maximum cascade fraction that could result in a non-detection of an angular extension. Uncertainties due to assumptions about the intrinsic spectra of the sources and the EBL model used in the cascade simulation were considered. The impact of these uncertainties is significant, but it was still possible to rule out a range of IGMF strengths around 10^{-16} G to 10^{-15} G at the 99% confidence level, assuming a correlation length of 1 Mpc.

VERITAS produced a complementary result to the H.E.S.S. measurement, and arrived at similar conclusions (Archambault, S. and others, 2017). Observations of seven hard-spectrum blazars were utilized, covering a range of redshifts from $z = 0.031$ to $z \sim 0.5$. As with the H.E.S.S. measurement, the angularly extended flux was constrained to be less than a few percent of the Crab nebula flux. One source (1ES 1218+304) was found to be the most useful object for IGMF studies, due to its brightness, redshift, and hard intrinsic spectrum with no identified cutoff. It was thus the only source considered for extracting IGMF limits. Limits on the cascade fraction as a function of IGMF strength were set, and used to constrain the IGMF strength. The choice of sources makes the H.E.S.S. and VERITAS measurements overlapping but complementary, with VERITAS ruling out a set of slightly stronger IGMF strengths between 10^{-15} G and 10^{-14} G at the 95% confidence level, assuming a correlation length of 1 Mpc.

The definitive study, at the time of writing, is a search that combined angular and spectral information from *Fermi*-LAT data and archival IACT spectra (Fermi-LAT Collaboration et al., 2018b), with the spectral information proving key to the extraction of IGMF constraints. A set of six hard-spectrum blazars, with low detected variability and spectral points extending to an optical depth $\tau = 2$ were studied individually, as well as jointly in a stacked analysis. The time period for which the sources were assumed to be active was varied from 10 to 10^7 years, the former corresponding to the observation period and the latter to the typical AGN activity timescale, and the IGMF constraints re-evaluated. Even in the case of the most conservative assumption of the blazars only being active for 10 years, the extracted limits were significantly more constraining than the other measurements discussed here. A lower limit of $B \gtrsim 10^{-16}$ G was set at the 95%

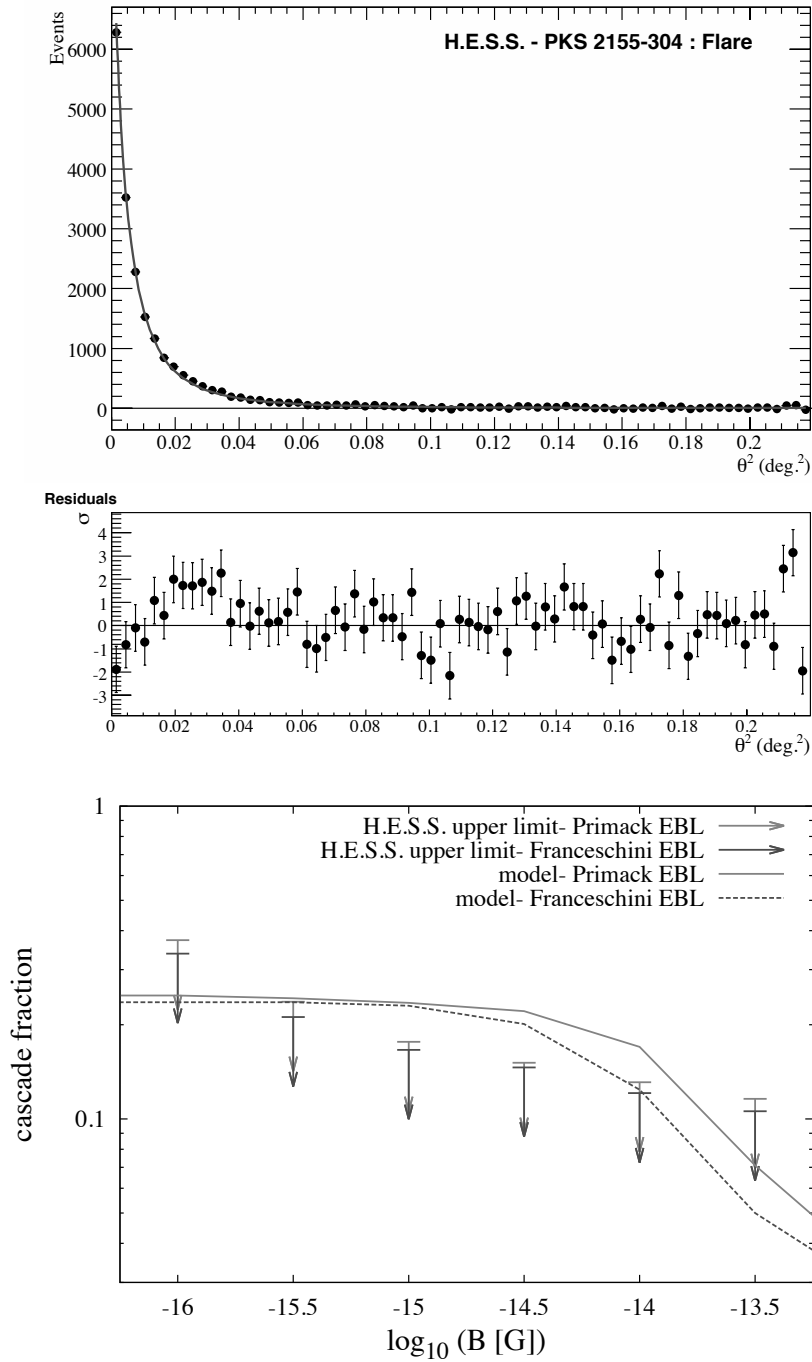


Figure 7.7: The top panel shows the angular profile of a flaring blazar observed by H.E.S.S. (shown as data point), whose angular extension is expected to be only due to the instrument point spread function. It is in good agreement with a simulated point source (solid line). In the bottom panel, upper limits on the observed cascade fraction are compared against predictions, as a function of IGMF strength. Figure extracted from [Abramowski et al. \(2014\)](#).

confidence level, assuming a correlation length greater than 10 kpc. Combined with the smaller H.E.S.S. and VERITAS exclusion regions, the *Fermi*-LAT results substantially reduce the allowed region for a weak IGMF.

7.2.5 Relation to non-VHE measurements

As is shown in Fig. 7.5, upper limits on the IGMF strength are also available based on non-VHE measurements (Heiles and Troland, 2004). Magnetic fields encountered en route to the observer lead to Zeeman splitting of the 21 cm hydrogen absorption line in quasar spectra. The primary expected contributor to this is the Galactic magnetic field, thus the IGMF must clearly be less than the total magnetic field derived from Zeeman splitting (Neronov and Semikoz, 2009). Another constraint comes from polarized emission from quasars, which undergoes Faraday rotation. The polarization angle of the emission changes with wavelength, with the ratio of the change in polarization to the change in wavelength varying directly with the magnetic-field strength along the line of sight (Blasi et al., 1999). Lastly, tangled primordial magnetic fields are expected to produce anisotropies in the CMB, the non-observation of which can be used to constrain the field strength (Ade et al., 2015, 2016b, Jedamzik and Saveliev, 2019). Further constraints can be derived from Big Bang nucleosynthesis, namely that a large primordial magnetic field would drive a too-fast expansion of the universe, slowing heavy-element formation and leading to a greater fraction of hydrogen to heavy elements than is observed (Grasso and Rubinstein, 2001).

Upper limits on the IGMF correlation length are set under the assumption that the correlation length must be less than the size of the universe, while lower limits on the correlation length can be set based on the predicted decay time of the IGMF due to magnetic diffusion.

In addition to its interest as a cosmological observable, the IGMF strength and structure is experimentally relevant for a number of measurements. Ultra-high-energy cosmic rays are bent by the IGMF, although the effect of magnetic fields in voids is expected to be subdominant compared to deflections by the stronger magnetic fields in filaments, galaxy clusters and in the Milky Way. As discussed in the chapter dedicated to fundamental physics, the IGMF is also important for studies of axion-like particles, hypothetical particles which couple to the magnetic field, converting to and from VHE photons (Doro et al., 2021).

7.2.6 Outlook

Magnetism on cosmological scales remains a mystery. As discussed in the introduction, lower limits on the IGMF strength based on the Harrison effect are nearly fifteen orders of magnitude too low to explain the missing cascade component at low gamma-ray energies. Is the IGMF strength larger than constrained by H.E.S.S. and VERITAS? Which magnetic-field generation scenarios are the most viable and what would be the resulting strength, correlation length, and helicity of the IGMF in voids today? Could plasma instabilities play a significant role in cooling electron-positron beams that develop over dozens of Mpc?

More precise non-VHE measurements and convincing theoretical arguments may reduce the allowed region for the IGMF strength and correlation length, and further study of collective plasma effects may clarify predictions for the cascade development. However, observational searches with IACTs have already shown the possibility to probe an uncharted territory in the parameter space of the IGMF. These searches can be expected to expand beyond blazar-based studies in the coming years, as a catalog of TeV-detected GRBs is assembled, enabling a parallel set of searches. As-

sociations between neutrinos and blazars, discussed in the chapter dedicated to multi-messenger astronomy, also present a potentially promising route to constrain the IGMF, using the time delay between the neutrino measurement and gamma-ray flare detection.

Regardless of the source class considered in IGMF searches, a low energy threshold, sensitivity from tenths to tens of TeV to constrain both the primary and secondary components, and an angular resolution at the few arcminute level constitute the key characteristics of an instrument that will be able to either measure for the first time or strongly constrain the large-scale magnetism of the universe. With these capabilities, CTA will probe IGMF strengths up to 0.3 pG (CTA Consortium et al., 2021). Future VHE gamma-ray observations will doubtless improve our understanding of the origin of cosmic magnetism.

7.3 Lorentz invariance violation

We now turn to a topic focussed on the fundamental physical laws of the universe rather than its evolution. Lorentz invariance and the constancy of the speed of light c for all inertial observers underpin the current understanding of relativity and quantum mechanics. A number of theories that attempt to unite gravity with the other fundamental forces and incorporate it into a quantum mechanical framework predict violation of Lorentz invariance at or below the Planck scale, $E_{\text{Pl}} \approx 1.22 \times 10^{19}$ GeV (e.g. Rovelli, 2008). This prediction can be tested with gamma-ray astronomy (see e.g. Amelino-Camelia, 2013, Amelino-Camelia and Smolin, 2009, Ellis et al., 2008 and references therein). Such theories are most simply expressed in terms of effective field theories, with two consequences. First, general and special relativity are recovered at leading order of the Lagrangian, but higher-order terms, scaling with powers of the energy, appear in the Lagrangian. Second, the effective field theory breaks down at a specific energy, presumably below the Planck scale. These consequences dictate the search strategy and energy scale of interest in the measurements described below. Observations can be used to constrain particular effective field theories (see e.g. Kislat and Krawczynski, 2015, where constraints are placed on a specific model, the Standard Model Extension), but the approach taken in most studies has been simpler: to set a lower limit on the energy scale at which a modification to Lorentz invariance can occur.

7.3.1 Theoretical framework

A natural consequence of quantum gravity is that the uncertainty principle makes the vacuum richer (“fuzzy” or “foamy”). This introduces a small refractive index for particles travelling through the vacuum, resulting in an energy-dependent dispersion.

Rather than the classic relation $E^2 = p^2c^2 + m^2c^4$, the energy in effective field theories incorporating LIV can be generically expanded as

$$E^2 = p^2c^2 + m^2c^4 \pm E^2 \left(\frac{E}{\xi_n E_{\text{LIV}}} \right)^n \quad (7.10)$$

where c is the standard speed of light, E_{LIV} sets the energy scale of the modifications, and the coefficients ξ_n give the relative size of the terms in the expansion (note that ξ_n can be very large/infinite, rendering terms negligible/zero). The additional terms can be positive or negative, corresponding to a superluminal or subluminal velocity, respectively. The latter is generally considered more theoretically probable (Jacob and Piran, 2008). It should be noted that odd-powered terms violate

CPT invariance (charge conjugation/parity/time, where parity refers to a spatial inversion), and thus theories that respect CPT will only contain even-powered terms. However, while the standard model of particle physics respects CPT, it can be violated in models incorporating LIV [Amelino-Camelia \(2013\)](#).

7.3.2 VHE observables

Gamma rays travelling over large distances will accumulate effects of Lorentz Invariance Violation (LIV), and the agreement between their expected and observed propagation provides a probe of modifications at a given energy scale. This is of particular interest as it is an energy regime that cannot be tested with the particle physics experiments upon which we base our understanding of quantum mechanics and special relativity.

Modification of pair-production threshold

Returning to the earlier discussion of the EBL, the energy threshold for pair production of gamma rays interacting with EBL photons is modified by LIV terms ([Jacob and Piran, 2008](#), [Kifune, 1999](#)). Assuming energy/momentum conservation and considering all particle types to be equally affected by LIV, this modifies Eq. (7.1) for the subluminal case to

$$E'_\gamma \epsilon'_{\text{EBL}} \geq (m_e c^2)^2 + \frac{1 - 2^{-n}}{4} \left(\frac{E'_\gamma}{\xi_n E_{\text{LIV}}} \right)^n E'^2_\gamma \quad (7.11)$$

It can be seen from Eq. (7.11) that LIV raises the energy threshold for pair production for a subluminal modification of the dispersion relation. As shown in Fig. 7.8, subluminal LIV decreases the opacity of the universe to gamma rays, by effectively depleting the target photon field interacting with gamma rays above 10 TeV. Assuming that the pair-production cross section retains its functional dependence on energy under LIV, the loss and recovery of transparency are nearly symmetric around a critical energy ([Jacob and Piran, 2008](#)), as shown in Fig. 7.8. As the effect is most noticeable at the highest energies in a gamma-ray spectrum, tests of LIV-induced threshold modifications are best performed using observations of blazars with hard photon spectra extending to tens of TeV.

Energy-dependent time dispersion

Another approach to searching for LIV, which requires no assumptions about kinematics, is to search for a correlation between the energy and arrival time of gamma rays. In this case, the limiting assumption is that all of the gamma rays were produced at the same time at the source (we will discuss the uncertainties associated with this assumption below). For an individual photon, a subluminal modification to the velocity is parametrised as

$$v = c \times (1 - (E/\chi_n E_{\text{LIV}})^n) \quad (7.12)$$

The parameter χ_n is the equivalent ξ_n in Eq. (7.11) within a numerical factor. A more direct link between Eq. (7.11) and Eq. (7.12) can be found by defining the velocity following the formalism of Hamiltonian mechanics, that is, as $v = \partial E / \partial p$.

Measuring the arrival time of gamma rays of different energies coming from the same emitter enables the extraction of E_{LIV} . The limitation of this method is obvious: how does the observer

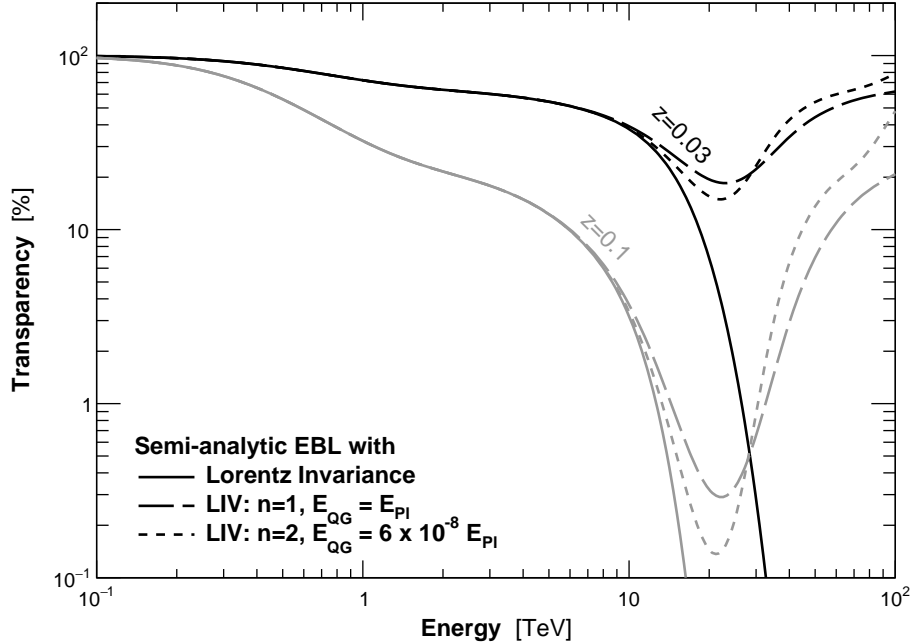


Figure 7.8: Attenuation factor, in percent, as a function of gamma-ray energy on Earth, for sources located at $z = 0.03$ and $z = 0.1$, following the semi-analytical EBL model of Gilmore et al. (2012) and the LIV formalism of Jacob and Piran (2008). Both linear ($n = 1$) and quadratic ($n = 2$) modifications of the pair-creation threshold are shown, at the Planck scale for $n = 1$, and at an ad-hoc energy scale of $6 \times 10^{-8} E_{\text{PI}}$ for $n = 2$, resulting in a similar effect.

know that the gamma rays were generated in the source at the same time? Such searches focus on bursts of gamma rays, whether from GRBs, AGN flares, or the well-defined flux peaks in pulsar lightcurves, where a sharp increase in flux occurs across the gamma-ray energy range. For single sources, this method remains vulnerable to intrinsic energy dependence of emission at the source (for instance, due to the presence of different emission regions), which could either increase or decrease the observed time dispersion.

A robust detection of an LIV effect would consequently rely on the combination of observations from multiple sources, and indeed multiple types of sources, located at different redshifts. The time difference due to LIV should increase as a function of redshift as the effects accumulate over the photon's path length. Detection of an energy-dependent dispersion without such a trend would point to intrinsic source effects.

In terms of source selection, the properties of GRBs, AGN, and pulsars offer different advantages and disadvantages. The ideal candidates for LIV studies are distant (LIV effects accumulate over distance), rapidly variable (producing well-defined bursts of gamma rays), and detected to high energies (as the modifications to the propagation scale with energy).

AGN and GRBs are attractive candidates for the first and third properties, located at cosmological distances and with energy spectra that are observed to extend to tens of TeV for AGN and beyond 1 TeV for GRBs. The flux variability of AGN is however not optimal, as it is unpredictable

and often slow (timescales of days to years). GRBs behave more predictably, with a rapid burst of gamma rays followed by a steep decay in the gamma-ray flux, but there is variation between bursts as well as uncertainty in the underlying structure of the flux as a function of time. Pulsars are excellent candidates from the perspective of flux variability. The peaks of their lightcurves are sharp and predictable (enabling improvements in statistical uncertainties of LIV tests by simply observing the sources for longer), and changes in their behaviour, due to e.g. spin-down, are precisely predicted. For energy range and distance, though, pulsars are less attractive candidates, located within our galaxy and emitting gamma rays to ~ 1 TeV rather than tens of TeV. Only four pulsars are detected at VHE; of these, the Crab pulsar is detected to the highest energies, up to ~ 1.5 TeV (Ansoldi, S. et al., 2016).

7.3.3 VHE constraints

Search for modification of pair-production threshold

The large blazar spectral sample of Biteau and Williams (2015) facilitated the extraction of limits on E_{LIV} , while leaving the EBL SED free within observational constraints. A range of possible E_{LIV} was scanned under the assumption of subluminal LIV, with a recalculation of the optical depth with the modified pair production threshold of Eq. (7.11). No significant evidence of LIV was observed. Consequently, a lower limit of $E_{\text{LIV}} > 0.6 \times E_{\text{Pl}}$ was set at the 99% confidence level. This can be translated into a limit of $4 \times 10^{-8} \times E_{\text{Pl}}$ for a second order modification (see Eq. (32) in Biteau and Williams, 2015).

Similarly, Lang et al., 2019 evaluated three distinct EBL models and selected the most promising spectra for detecting LIV effects from a sample of 111 archival AGN energy spectra. The final sample included 18 spectra from 6 blazars, dominated by bright and only moderately distant ($z < 0.2$) objects. The extracted limits on E_{LIV} for subluminal LIV are well above the Planck energy for the linear ($n = 1$) term of Eq. (7.10), with $E_{\text{LIV}} < 10 \times E_{\text{Pl}}$ excluded at the 95% confidence level. For the quadratic term, $E_{\text{LIV}} < 2 \times 10^{-7} \times E_{\text{Pl}}$ is excluded.

As for studies of the EBL, analyses exploiting archival data are not devoid of possible biases. In particular for LIV, the treatment of upper limits at the high-energy end of the gamma-ray spectra is expected to impact the constraining power on the LIV energy scale, which could contribute to the differences in the results from the two above-mentioned studies.

Search for energy-dependent time dispersion

In 2006, H.E.S.S. observed a massive flare from PKS 2155-304, peaking above 10 times the flux of the Crab Nebula. The source displayed significant variability on the time scale of minutes. A time-dependent analysis was performed wherein the structure of the intrinsic flux variability was assumed to be given by the observed flux variability of the lowest energy gamma rays, between 0.25 TeV and 0.28 TeV. No distortion of the lightcurve stage at higher energies was allowed, only an overall shift in arrival time.

No evidence for an energy-dependent time dispersion was observed, and lower limits were set on E_{LIV} : on the linear term at $0.2 \times E_{\text{Pl}}$, on the quadratic term at $5 \times 10^{-9} \times E_{\text{Pl}}$, both at the 95% confidence level. While these limits were calculated for the subluminal case, the superluminal case gives similar, slightly weaker limits (Abramowski et al., 2011).

A similar study was undertaken by MAGIC for two flares of the blazar Mrk 501, yielding similar limits for the quadratic term to the H.E.S.S. result, and order-of-magnitude weaker limits on the

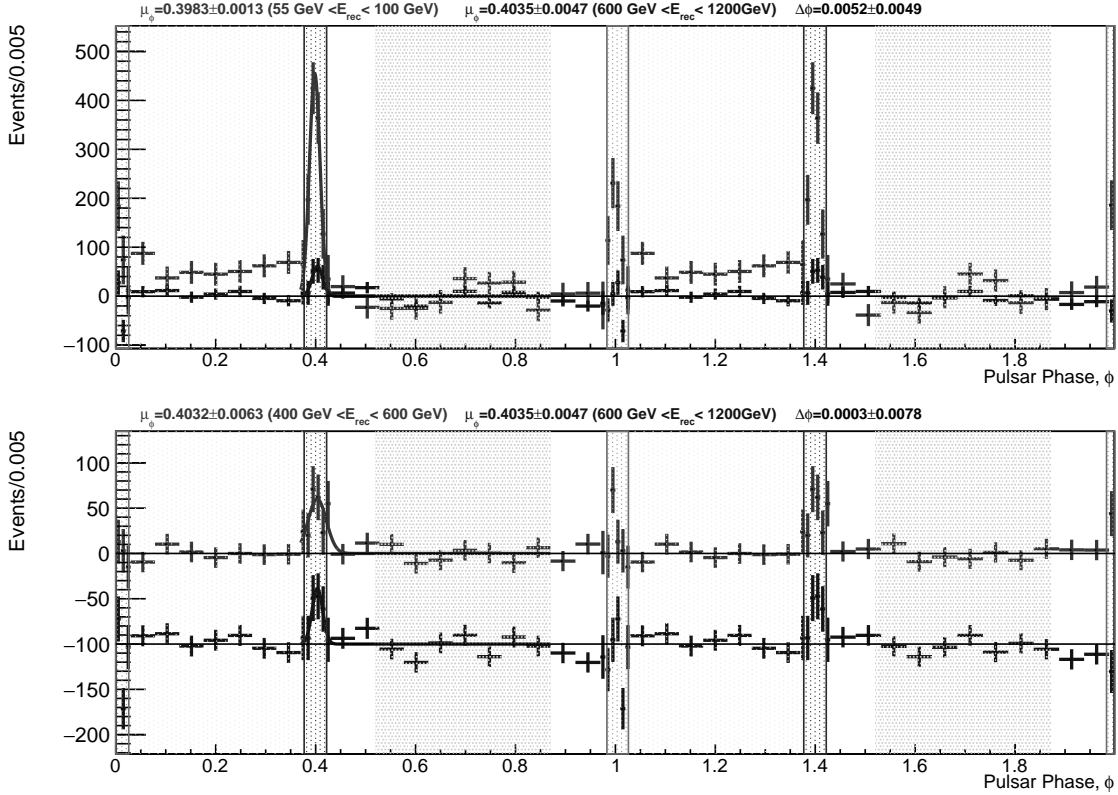


Figure 7.9: The Crab pulsar folded lightcurve as measured by MAGIC. Two periods are shown, for high and low gamma-ray energies. The shaded areas define the pulse and inter-pulse regions. Figure extracted from [Ahnen et al. \(2017\)](#).

linear term ([Albert et al., 2008](#), [Martínez and Errando, 2009](#)).

Turning to pulsars, the MAGIC collaboration produced LIV constraints based on 12 years of observations of the Crab pulsar ([Ahnen et al., 2017](#)). As a pulsar, its flux shows a predictable time structure, in the case of the Crab characterised by two sharp peaks of differing intensity, and a low state or non-detected state in between the peaks, as shown in Fig. 7.9. While the variability behaviour of the source is controlled, the distance to the Crab pulsar is to date only measured to 25% accuracy ([Kaplan et al., 2008](#)), which propagates to an uncertainty on the derived LIV results. Both a simple comparison of the peak positions in time for gamma rays in different energy ranges and a full likelihood analysis were performed, yielding consistent results. In the absence of an LIV signal, lower limits were calculated at the 95% confidence level for E_{LIV} , corresponding to $0.05 \times E_{\text{P1}}$ for the linear term and $5 \times 10^{-9} \times E_{\text{P1}}$ for the quadratic term, assuming subluminal LIV. As for the results of [Abramowski et al. \(2011\)](#), the limits for the superluminal case are slightly weaker.

With the detection of the first GRBs at VHE, a new source class is available for time dispersion measurements. In particular, the MAGIC-detected GRB190114C had the large redshift ($z \sim 0.4$) and high-energy photons (largest detected photon energy was ~ 2 TeV) necessary to produce competitive LIV constraints ([MAGIC Collaboration et al., 2020](#)). The dominant uncertainty in this measurement is the shape of the intrinsic emission as a function of time. The authors considered a minimal model, which assumes zero emission before the multiwavelength GRB alert was issued,

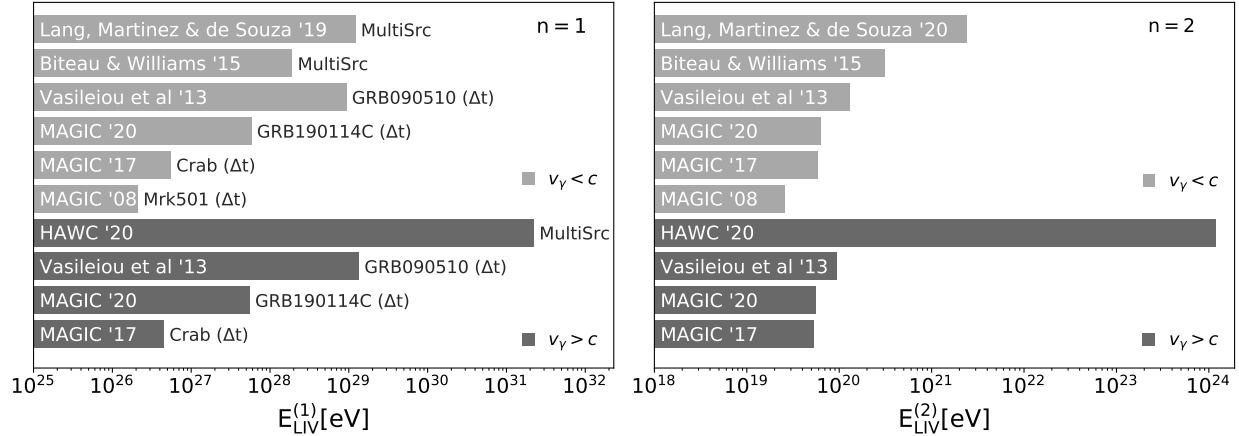


Figure 7.10: Summary of the lower limits on the energy scale of LIV, E_{LIV} . The left panel shows the limits on the linear term, the right panel on the quadratic term. Light grey bars assume a subluminal modification, while dark grey bars assume a superluminal modification. Credit: Humberto Martínez-Huerta, adapted from [Martínez-Huerta et al. \(2020\)](#).

triggering MAGIC observations, as well as a theoretically motivated model in which the peak emission occurs before the beginning of MAGIC observations. Neither model of the intrinsic emission provided evidence for LIV, and the extracted 95% confidence level limits were comparable, with $0.5 \times E_{P1}$ for the subluminal linear term, assuming the physically motivated emission model, and $5 \times 10^{-9} \times E_{P1}$ for the subluminal quadratic term. Such limits suggest a sensitivity similar to that of AGN time dispersion measurements: the lower energy of gamma rays from the GRB are compensated by the greater redshift of the source.

A summary of the limits discussed here, including the non-IACT measurements discussed in the next section, is given in Fig 7.10. Further discussion of current limits on LIV can be found in [Martínez-Huerta et al. \(2020\)](#).

7.3.4 Relation to non-IACT measurements

The most constraining limits on the subluminal linear term for LIV come from *Fermi*-LAT. These constraints are based on observations of GRBs, which within the *Fermi*-LAT sensitive energy range are ideal candidates, with sharp flux variability and broadband emission, and occurring at cosmological distances. A large sample of GRBs has been measured, although several of the canonical limits are from individual ([Abdo et al., 2009](#)) or small samples of GRBs ([Vasileiou et al., 2013](#)). However, GRBs exhibit intrinsic energy-dependent time lags which must be taken into account ([Ackermann et al., 2013](#)). Lower limits at the 95% confidence level on E_{LIV} exceed the Planck scale by a factor of 7.6 for the linear term, going down to a factor of 2 when accounting for systematic uncertainties related to emission processes at the source. For the quadratic term, the limits are comparable to many of the VHE limits, at $1 \times 10^{-8} \times E_{P1}$ ([Vasileiou et al., 2013](#)).

The HAWC observatory has strongly constrained superluminal LIV by searching for high-energy spectral cutoffs induced by photon decay to an electron/positron pair or to multiple photons ([HAWC Collaboration et al., 2020](#)). This search utilised four Galactic high-energy emitters, including the Crab Nebula, and placed 95% confidence level lower limits on E_{LIV} three orders of magnitude above

the Planck energy for the linear term and $7 \times 10^{-6} \times E_{\text{Pl}}$ on the quadratic term.

Upper limits on the flux of photons at ultra-high energies ($E > 10^{18}$ eV) might also provide stringent constraints on LIV, provided the sources are identified and a significant fraction of protons is present at the highest energies. Such a probe could reach the Planck scale even for second-order modification of the pair-creation threshold (Gelmini et al., 2008, Guedes Lang et al., 2018). LIV could also impact the spectrum of UHECR by increasing the threshold for photo-production of pions (see Sec. 3.5 in Amelino-Camelia, 2013 for an excellent review of the debates on this matter). The constraints on the composition and sources of UHECR expected from the upgrade of the Pierre Auger Observatory will help in determining the magnitude of the constraints on LIV from UHECR propagation.

7.3.5 Outlook

The violation of Lorentz invariance at energies beyond the reach of man-made accelerators can be studied with gamma rays at GeV-TeV energies. Two paths have been followed in the VHE regime, both based on phenomenological modifications of the dispersion relation of photons, resulting in high-energy correction terms.

Assuming that speed can be computed from Hamiltonian mechanics within a quantum-gravity framework, such modifications result in an energy-dependent speed of light, whose effect, cumulated over cosmological scales, could be observed as an energy-dependent time-lag between successive gamma-ray bands. The lack of such lags has already allowed ground-based instruments to place limits on the LIV energy scale that, for a linear modification, approach the Planck scale. The timing capabilities of CTA will be more than three orders of magnitude better than *Fermi*-LAT in the 30-100 GeV band (Funk and Hinton, 2013). This will facilitate the detection of numerous highly variable extragalactic sources (GRBs, blazars), constituting a gold mine for LIV studies.

An alternative approach, based on four-momentum conservation, suggests that LIV corrections should result in a modification of the pair-creation threshold, directly affecting the transparency of the universe beyond tens of TeV. In contrast to timing approaches, the limits for a linear modification have been quoted an order of magnitude above the Planck scale. However, limits on the subluminal quadratic modification, which is particularly motivated from the theoretical perspective, remain well below the Planck energy, on the order of $10^{-7} \times E_{\text{Pl}}$. Thanks to its enhanced sensitivity at the highest energies, CTA will be able to probe LIV predictions in both nearby (Fairbairn et al., 2014) and more distant objects (Tavecchio and Bonnoli, 2016), either improving existing constraints or finding evidence for LIV (CTA Consortium et al., 2021).

The two approaches, based on timing on the one hand and spectral reconstruction on the other, are complementary in their assumptions: the first assumes an energy-dependent modification in propagation time, the second a modification to the kinematics of pair production. The discovery of LIV in one channel does not demand it in the other. The surprise with CTA may come from studies of the second-order modification, which affects gamma-ray observables at an LIV energy scale beyond 10^{20} eV.

7.4 Status and prospects of TeV gamma-ray cosmology

In this chapter, we have attempted to demonstrate the relevance of VHE gamma-ray observations for understanding cosmology. We have examined time scales ranging from the Planck time to the current day, considering Lorentz invariance violation and cosmological magnetic and photon

fields. The current generation of IACTs has made progress in measuring or constraining all of these cosmological observables. We summarise by pointing out that gamma-ray-based measurements are beginning to probe EBL wavelengths where theoretical models developed prior to the gamma-ray detections disagree, are rapidly narrowing the allowed range of intergalactic magnetic field strength and correlation length, and are pushing the lower limit on the energy scale at which Lorentz invariance violation may occur beyond the Planck scale. We have also discussed the relevance of these measurements for other fields of astrophysics and astroparticle physics, particularly the spectral energy distribution of the diffuse supernova neutrino background and the propagation of UHECR. We have noted the extent to which the gamma-ray measurements are limited by astrophysical uncertainties, namely those associated with the production of VHE gamma rays in astrophysical sources. While current-generation IACTs have not made their final statements on the topics discussed above, we can look to CTA to substantially improve our knowledge and possibly make ground-breaking discoveries. The precise energy and angular resolution of CTA, coupled with its high flux sensitivity, will allow it to quickly supersede existing instruments, dramatically improving our understanding of the light content of the universe, cosmic magnetism, and the structure of space time.

Exercise 1

The energy density of the CMB at the present epoch is about $\rho_{\text{CMB}} \sim 0.26 \text{ eV cm}^{-3}$ and the integral cross section for pair production can be estimated to be $\sim \sigma_{\text{T}}/10$, where σ_{T} is the Thomson cross section. Gamma rays with energies around 1 TeV mostly interact with photons from COB.

1. Estimate the energy density of COB photons, using the information given in the text about the relative budgets of the CMB and EBL.
2. Modeling the EBL spectrum as a Dirac function peaked at 1 eV, and noting that 1 TeV gamma rays pair produce mainly with 1 eV photons, compute the optical depth, τ , for 1 TeV gamma rays as a function of distance $L \sim cz/H_0$ (valid for $z \ll 1$) in Gpc.
3. Where is the cosmic gamma-ray horizon, defined as the distance for which $\tau = 1$, located for 1 TeV gamma rays?

Note: The cosmic gamma-ray horizon for 1 TeV gamma rays is typically reached for sources at $z \sim 0.1$, check if the value of the corresponding luminosity distance is consistent with your rough estimate.

- List of constants -

- $\sigma_{\text{T}} \sim 6.6 \times 10^{-25} \text{ cm}^2$
- $1 \text{ pc} \sim 3.1 \times 10^{18} \text{ cm}$

Exercise 2

The total pair-production cross section, under the assumption of an isotropic distribution of EBL photons, can be approximated by (Coppi and Blandford, 1990):

$$\sigma(x) = \sigma_0 \times \frac{x^2 - 1}{x^3} \ln x \quad \text{for } x > 1 \quad (13)$$

where $x = E_{\gamma} \epsilon_{\text{EBL}}$ is the product of the energies of the gamma ray and of the EBL photon.

1. Locate numerically the maximum of the total pair-production cross section.
2. Compute the wavelength of EBL photons which are most likely to interact with 0.1, 1, and 10 TeV gamma rays.

- List of constants -

- $\hbar c \sim 197 \text{ MeV fm}$

Exercise 3

Electrons and positrons produced by the interaction of gamma rays with EBL photons can inverse Compton scatter on CMB photons, boosting them to higher energies. In the Thomson regime (the low-energy limit of Compton scattering), the average energy of the secondary gamma rays is:

$$E_\gamma = \frac{4}{3}\gamma_e^2\epsilon_{\text{CMB}} \quad (14)$$

where $\epsilon_{\text{CMB}} \sim 0.6 \text{ meV}$ is the average CMB photon energy, and where γ_e is the Lorentz factor of the electron/positron.

1. The Thomson regime is defined as $\gamma_e\epsilon_{\text{CMB}} \ll m_e c^2$. Up to which electron Lorentz factor is Eq. (14) valid?
2. Compute the energy of the secondary gamma rays for primary photons at 0.2, 2, and 20 TeV.

Exercise 4

Phenomenological modifications to the dispersion relation of particles at high energies can be written as :

$$E^2 = p^2 c^2 + m^2 c^4 \pm E^2 \left(\frac{E}{\xi_n E_{\text{LIV}}} \right)^n \quad (15)$$

where E_{LIV} is the energy scale at which Lorentz invariance violation appears and n is the order of the correction. In a Hamiltonian formalism where $v = \partial E / \partial p$, this results in subluminal/superluminal motion of particles.

1. Show that to order n , for $m \ll E \ll E_{\text{LIV}}$: $v = c \times (1 \pm (E/\chi_n E_{\text{LIV}})^n)$, with $\chi_n = \left(\frac{n+1}{2}\right)^{-n} \xi_n$
2. Compare the relative size of the coefficients giving the LIV scale obtained from time delays and threshold effects for first and second-order modifications of the dispersion relation.

Bibliography

- H. Abdalla et al. Measurement of the EBL spectral energy distribution using the VHE γ -ray spectra of H.E.S.S. blazars. *A&A*, 606:A59, Oct. 2017. doi: 10.1051/0004-6361/201731200.
- A. A. Abdo et al. A limit on the variation of the speed of light arising from quantum gravity effects. *Nature*, 462:331–334, Nov. 2009. doi: 10.1038/nature08574.
- A. U. Abeysekara et al. Gamma-Rays from the Quasar PKS 1441+25: Story of an Escape. *ApJL*, 815:L22, Dec. 2015. doi: 10.1088/2041-8205/815/2/L22.
- A. Abramowski et al. Search for Lorentz Invariance breaking with a likelihood fit of the PKS 2155-304 Flare Data Taken on MJD 53944. *Astrop. Phys.*, 34:738–747, 2011. doi: 10.1016/j.astropartphys.2011.01.007.
- A. Abramowski et al. Measurement of the extragalactic background light imprint on the spectra of the brightest blazars observed with H.E.S.S. *A&A*, 550:A4, Feb. 2013. doi: 10.1051/0004-6361/201220355.
- A. Abramowski et al. Search for extended γ -ray emission around AGN with H.E.S.S. and Fermi-LAT. *A&A*, 562:A145, Feb. 2014. doi: 10.1051/0004-6361/201322510.
- M. Ackermann et al. The Imprint of the Extragalactic Background Light in the Gamma-Ray Spectra of Blazars. *Science*, 338:1190, Nov. 2012. doi: 10.1126/science.1227160.
- M. Ackermann et al. The First Fermi-LAT Gamma-Ray Burst Catalog. *ApJS*, 209:11, Nov. 2013. doi: 10.1088/0067-0049/209/1/11.
- P. A. R. Ade et al. POLARBEAR constraints on cosmic birefringence and primordial magnetic fields. *Phys. Rev. D*, 92:123509, Dec 2015. doi: 10.1103/PhysRevD.92.123509.
- P. A. R. Ade et al. Planck 2015 results. XIII. Cosmological parameters. *A&A*, 594:A13, Sept. 2016a. doi: 10.1051/0004-6361/201525830.
- P. A. R. Ade et al. Planck 2015 results. XIX. Constraints on primordial magnetic fields. *A&A*, 594:A19, Sept. 2016b. doi: 10.1051/0004-6361/201525821.
- F. A. Aharonian et al. An Exceptional Very High Energy Gamma-Ray Flare of PKS 2155-304. *ApJL*, 664:L71–L74, Aug. 2007. doi: 10.1086/520635.
- M. L. Ahnen et al. Detection of very high energy gamma-ray emission from the gravitationally lensed blazar QSO B0218+357 with the MAGIC telescopes. *A&A*, 595:A98, Nov. 2016. doi: 10.1051/0004-6361/201629461.

- M. L. Ahnen et al. Constraining Lorentz Invariance Violation Using the Crab Pulsar Emission Observed up to TeV Energies by MAGIC. *ApJS*, 232:9, Sept. 2017. doi: 10.3847/1538-4365/aa8404.
- J. Albert et al. Probing quantum gravity using photons from a flare of the active galactic nucleus Markarian 501 observed by the MAGIC telescope. *Phys. Let. B*, 668:253–257, Oct. 2008. doi: 10.1016/j.physletb.2008.08.053.
- J. Aleksić et al. Search for an extended VHE γ -ray emission from Mrk 421 and Mrk 501 with the MAGIC Telescope. *A&A*, 524:A77, Dec. 2010. doi: 10.1051/0004-6361/201014747.
- J. Aleksić et al. Very High Energy γ -Rays from the Universe’s Middle Age: Detection of the $z = 0.940$ Blazar PKS 1441+25 with MAGIC. *ApJL*, 815:L23, Dec. 2015. doi: 10.1088/2041-8205/815/2/L23.
- R. Alves Batista and A. Saveliev. The Gamma-Ray Window to Intergalactic Magnetism. *Universe*, 7(7):223, July 2021. doi: 10.3390/universe7070223.
- R. Alves Batista et al. Effects of uncertainties in simulations of extragalactic UHECR propagation, using CRPropa and SimProp. *J. Cosmology Astropart. Phys.*, 10:063, Oct. 2015. doi: 10.1088/1475-7516/2015/10/063.
- R. Alves Batista et al. CRPropa 3-a public astrophysical simulation framework for propagating extraterrestrial ultra-high energy particles. *J. Cosmology Astropart. Phys.*, 2016(05):038, 2016.
- G. Amelino-Camelia. Quantum-Spacetime Phenomenology. *Living Reviews in Relativity*, 16:5, June 2013. doi: 10.12942/lrr-2013-5.
- G. Amelino-Camelia and L. Smolin. Prospects for constraining quantum gravity dispersion with near term observations. *Phys. Rev. D*, 80:084017, Oct 2009. doi: 10.1103/PhysRevD.80.084017.
- S. K. Andrews, S. P. Driver, L. J. M. Davies, C. d. P. Lagos, and A. S. G. Robotham. Modelling the cosmic spectral energy distribution and extragalactic background light over all time. *MNRAS*, 474:898–916, Feb. 2018. doi: 10.1093/mnras/stx2843.
- Ansoldi, S. et al. Teraelectronvolt pulsed emission from the Crab Pulsar detected by MAGIC. *A&A*, 585:A133, 2016. doi: 10.1051/0004-6361/201526853. URL <https://doi.org/10.1051/0004-6361/201526853>.
- Archambault, S. and others . Search for Magnetically Broadened Cascade Emission from Blazars with VERITAS. *ApJ*, 835:288, Feb. 2017. doi: 10.3847/1538-4357/835/2/288.
- T. C. Arlen et al. Intergalactic Magnetic Fields and Gamma-Ray Observations of Extreme TeV Blazars. *ApJ*, 796:18, Nov. 2014. doi: 10.1088/0004-637X/796/1/18.
- A. Barrau, A. Gorecki, and J. Grain. An original constraint on the Hubble constant: $h > 0.74$. *MNRAS*, 389(2):919–924, Sept. 2008. doi: 10.1111/j.1365-2966.2008.13607.x.
- J. Biteau and D. A. Williams. The Extragalactic Background Light, the Hubble Constant, and Anomalies: Conclusions from 20 Years of TeV Gamma-ray Observations. *ApJ*, 812(1):60, Oct. 2015. doi: 10.1088/0004-637X/812/1/60.

- J. Biteau et al. Progress in unveiling extreme particle acceleration in persistent astrophysical jets. *Nature Astronomy*, 4:124–131, Feb. 2020. doi: 10.1038/s41550-019-0988-4.
- O. Blanch and M. Martinez. Exploring the gamma ray horizon with the next generation of gamma ray telescopes. part 1: Theoretical predictions. *Astroparticle Physics*, 23(6):588 – 597, 2005a. ISSN 0927-6505. doi: <https://doi.org/10.1016/j.astropartphys.2005.03.008>. URL <http://www.sciencedirect.com/science/article/pii/S0927650505000642>.
- O. Blanch and M. Martinez. Exploring the gamma-ray horizon with the next generation of gamma-ray telescopes. part 2: Extracting cosmological parameters from the observation of gamma-ray sources. *Astroparticle Physics*, 23(6):598 – 607, 2005b. ISSN 0927-6505. doi: <https://doi.org/10.1016/j.astropartphys.2005.03.009>. URL <http://www.sciencedirect.com/science/article/pii/S0927650505000630>.
- O. Blanch and M. Martinez. Exploring the gamma ray horizon with the next generation of gamma ray telescopes. part 3: Optimizing the observation schedule of gamma ray sources for the extraction of cosmological parameters. *Astroparticle Physics*, 23(6):608 – 615, 2005c. ISSN 0927-6505. doi: <https://doi.org/10.1016/j.astropartphys.2005.03.010>. URL <http://www.sciencedirect.com/science/article/pii/S0927650505000629>.
- P. Blasi, S. Burles, and A. V. Olinto. Cosmological Magnetic Field Limits in an Inhomogeneous Universe. *ApJL*, 514:L79–L82, Apr. 1999. doi: 10.1086/311958.
- A. E. Broderick, P. Chang, and C. Pfrommer. The Cosmological Impact of Luminous TeV Blazars. I. Implications of Plasma Instabilities for the Intergalactic Magnetic Field and Extragalactic Gamma-Ray Background. *ApJ*, 752:22, June 2012. doi: 10.1088/0004-637X/752/1/22.
- P. S. Coppi and R. D. Blandford. Reaction rates and energy distributions for elementary processes in relativistic pair plasmas. *MNRAS*, 245:453–507, Aug. 1990.
- CTA Consortium, H. Abdalla, et al. Sensitivity of the Cherenkov Telescope Array for probing cosmology and fundamental physics with gamma-ray propagation. *J. Cosmology Astropart. Phys.*, 2021(2):048, Feb. 2021. doi: 10.1088/1475-7516/2021/02/048.
- C. D. Dermer et al. Time Delay of Cascade Radiation for TeV Blazars and the Measurement of the Intergalactic Magnetic Field. *ApJL*, 733:L21, June 2011. doi: 10.1088/2041-8205/733/2/L21.
- A. Desai et al. A GeV-TeV Measurement of the Extragalactic Background Light. *ApJL*, 874(1):L7, Mar. 2019. doi: 10.3847/2041-8213/ab0c10.
- E. Di Valentino et al. In the realm of the Hubble tension—a review of solutions. *Classical and Quantum Gravity*, 38(15):153001, July 2021. doi: 10.1088/1361-6382/ac086d.
- A. Domínguez and F. Prada. Measurement of the Expansion Rate of the Universe from γ -Ray Attenuation. *ApJL*, 771:L34, July 2013. doi: 10.1088/2041-8205/771/2/L34.
- A. Domínguez, J. D. Finke, F. Prada, J. R. Primack, F. S. Kitaura, B. Siana, and D. Paneque. Detection of the Cosmic γ -Ray Horizon from Multiwavelength Observations of Blazars. *ApJ*, 770:77, June 2013. doi: 10.1088/0004-637X/770/1/77.

- A. Domínguez et al. Extragalactic background light inferred from AEGIS galaxy-SED-type fractions. *MNRAS*, 410:2556–2578, Feb. 2011. doi: 10.1111/j.1365-2966.2010.17631.x.
- A. Domínguez et al. A New Measurement of the Hubble Constant and Matter Content of the Universe Using Extragalactic Background Light γ -Ray Attenuation. *ApJ*, 885(2):137, Nov. 2019. doi: 10.3847/1538-4357/ab4a0e.
- M. Doro, M. A. Sánchez-Conde, and M. Hütten. Fundamental Physics Searches with IACTs. 2021. URL <https://arxiv.org/abs/2111.01198>.
- S. P. Driver. Measuring energy production in the Universe over all wavelengths and all time. *arXiv e-prints*, art. arXiv:2102.12089, Feb. 2021.
- S. P. Driver et al. Measurements of Extragalactic Background Light from the Far UV to the Far IR from Deep Ground- and Space-based Galaxy Counts. *ApJ*, 827:108, Aug. 2016. doi: 10.3847/0004-637X/827/2/108.
- S. Duivenvoorden et al. Have we seen all the galaxies that comprise the cosmic infrared background at $250 \mu\text{m} \leq \lambda \leq 500 \mu\text{m}$? *MNRAS*, 491(1):1355–1368, Jan. 2020. doi: 10.1093/mnras/stz3110.
- R. Durrer and A. Neronov. Cosmological magnetic fields: their generation, evolution and observation. *A&A Rev.*, 21:62, June 2013. doi: 10.1007/s00159-013-0062-7.
- E. Dwek and F. Krennrich. The extragalactic background light and the gamma-ray opacity of the universe. *Astrop. Phys.*, 43:112–133, Mar. 2013. doi: 10.1016/j.astropartphys.2012.09.003.
- E. Dwek, R. G. Arendt, and F. Krennrich. The Near-Infrared Background: Interplanetary Dust or Primordial Stars? *ApJ*, 635(2):784, 2005.
- J. Ellis, N. Mavromatos, and D. Nanopoulos. Derivation of a vacuum refractive index in a stringy space-time foam model. *Physics Letters B*, 665(5):412 – 417, 2008. ISSN 0370-2693. doi: <https://doi.org/10.1016/j.physletb.2008.06.029>.
- A. Eungwanichayapant and F. Aharonian. Very High Energy Gamma Rays from e^\pm Pair Halos. *Int. J. of Mod. Phys. D*, 18:911–927, 2009. doi: 10.1142/S0218271809014832.
- M. Fairbairn et al. The CTA sensitivity to Lorentz-violating effects on the gamma-ray horizon. *J. Cosmology Astropart. Phys.*, 6:005, June 2014. doi: 10.1088/1475-7516/2014/06/005.
- Fermi-LAT Collaboration, S. Abdollahi, et al. A gamma-ray determination of the Universe’s star formation history. *Science*, 362(6418):1031–1034, Nov. 2018a. doi: 10.1126/science.aat8123.
- Fermi-LAT Collaboration, M. Ackermann, et al. The Search for Spatial Extension in High-latitude Sources Detected by the Fermi Large Area Telescope. *ApJS*, 237(2):32, Aug. 2018b. doi: 10.3847/1538-4365/aacdf7.
- J. D. Finke, S. Razzaque, and C. D. Dermer. Modeling the Extragalactic Background Light from Stars and Dust. *ApJ*, 712:238–249, Mar. 2010. doi: 10.1088/0004-637X/712/1/238.
- J. D. Finke et al. Constraints on the Intergalactic Magnetic Field with Gamma-Ray Observations of Blazars. *ApJ*, 814:20, Nov. 2015. doi: 10.1088/0004-637X/814/1/20.

- T. Fitoussi et al. Physics of cosmological cascades and observable properties. *MNRAS*, 466(3):3472–3487, 2017. doi: 10.1093/mnras/stw3365. URL <http://dx.doi.org/10.1093/mnras/stw3365>.
- A. Franceschini. Photon-Photon Interactions and the Opacity of the Universe in Gamma Rays. *Universe*, 7(5):146, May 2021. doi: 10.3390/universe7050146.
- A. Franceschini and G. Rodighiero. The extragalactic background light revisited and the cosmic photon-photon opacity. *A&A*, 603:A34, July 2017. doi: 10.1051/0004-6361/201629684.
- A. Franceschini, G. Rodighiero, and M. Vaccari. Extragalactic optical-infrared background radiation, its time evolution and the cosmic photon-photon opacity. *A&A*, 487:837–852, Sept. 2008. doi: 10.1051/0004-6361:200809691.
- S. Funk and J. A. Hinton. Comparison of Fermi-LAT and CTA in the region between 10-100 GeV. *Astrop. Phys.*, 43:348–355, Mar. 2013. doi: 10.1016/j.astropartphys.2012.05.018.
- G. B. Gelmini, O. E. Kalashev, and D. V. Semikoz. GZK photons as ultra-high-energy cosmic rays. *Soviet Journal of Experimental and Theoretical Physics*, 106:1061–1082, June 2008. doi: 10.1134/S106377610806006X.
- R. C. Gilmore. Constraining the near-infrared background light from Population III stars using high-redshift gamma-ray sources. *MNRAS*, 420:800–809, Feb. 2012. doi: 10.1111/j.1365-2966.2011.20092.x.
- R. C. Gilmore, R. S. Somerville, J. R. Primack, and A. Domínguez. Semi-analytic modelling of the extragalactic background light and consequences for extragalactic gamma-ray spectra. *MNRAS*, 422:3189–3207, June 2012. doi: 10.1111/j.1365-2966.2012.20841.x.
- R. J. Gould and G. P. Schröder. Pair Production in Photon-Photon Collisions. *Physical Review*, 155:1404–1407, Mar. 1967a. doi: 10.1103/PhysRev.155.1404.
- R. J. Gould and G. P. Schröder. Opacity of the Universe to High-Energy Photons. *Physical Review*, 155:1408–1411, Mar. 1967b. doi: 10.1103/PhysRev.155.1408.
- D. Grasso and H. R. Rubinstein. Magnetic fields in the early Universe. *Phys. Rep.*, 348:163–266, July 2001. doi: 10.1016/S0370-1573(00)00110-1.
- R. Guedes Lang, H. Martínez-Huerta, and V. de Souza. Limits on the Lorentz Invariance Violation from UHECR Astrophysics. *ApJ*, 853:23, Jan. 2018. doi: 10.3847/1538-4357/aa9f2c.
- H. E. S. S. Collaboration, H. Abdalla, et al. A very-high-energy component deep in the γ -ray burst afterglow. *Nature*, 575(7783):464–467, Nov. 2019. doi: 10.1038/s41586-019-1743-9.
- H. E. S. S. Collaboration, H. Abdalla, et al. Revealing x-ray and gamma ray temporal and spectral similarities in the GRB 190829A afterglow. *Science*, 372(6546):1081–1085, June 2021. doi: 10.1126/science.abe8560.
- E. R. Harrison. Generation of Magnetic Fields in the Radiation ERA. *Monthly Notices of the Royal Astronomical Society*, 147(3):279–286, 1970. doi: 10.1093/mnras/147.3.279. URL <http://dx.doi.org/10.1093/mnras/147.3.279>.

- HAWC Collaboration, A. Albert, et al. Constraints on Lorentz Invariance Violation from HAWC Observations of Gamma Rays above 100 TeV. *Phys. Rev. Lett.*, 124:131101, Mar 2020. doi: 10.1103/PhysRevLett.124.131101. URL <https://link.aps.org/doi/10.1103/PhysRevLett.124.131101>.
- C. Heiles and T. H. Troland. The Millennium Arecibo 21 Centimeter Absorption-Line Survey. III. Techniques for Spectral Polarization and Results for Stokes V. *ApJS*, 151:271–297, Apr. 2004. doi: 10.1086/381753.
- S. Horiuchi, J. F. Beacom, and E. Dwek. Diffuse supernova neutrino background is detectable in Super-Kamiokande. *Phys. Rev. D*, 79(8):083013, Apr. 2009. doi: 10.1103/PhysRevD.79.083013.
- U. Jacob and T. Piran. Inspecting absorption in the spectra of extra-galactic gamma-ray sources for insight into Lorentz invariance violation. *Phys. Rev. D*, 78(12):124010, Dec. 2008. doi: 10.1103/PhysRevD.78.124010.
- K. Jedamzik and A. Saveliev. Stringent Limit on Primordial Magnetic Fields from the Cosmic Microwave Background Radiation. *Phys. Rev. Lett.*, 123:021301, Jul 2019. doi: 10.1103/PhysRevLett.123.021301. URL <https://link.aps.org/doi/10.1103/PhysRevLett.123.021301>.
- M. Kachelriess, S. Ostapchenko, and R. Tomas. ELMAG: A Monte Carlo simulation of electromagnetic cascades on the extragalactic background light and in magnetic fields. *Computer Physics Communications*, 183(4):1036 – 1043, 2012. ISSN 0010-4655. doi: <https://doi.org/10.1016/j.cpc.2011.12.025>.
- T. Kahniashvili, A. Brandenburg, and A. G. Tevzadze. The evolution of primordial magnetic fields since their generation. *Physica Scripta*, 91(10):104008, Oct. 2016. doi: 10.1088/0031-8949/91/10/104008.
- D. L. Kaplan, S. Chatterjee, B. M. Gaensler, and J. Anderson. A Precise Proper Motion for the Crab Pulsar, and the Difficulty of Testing Spin-Kick Alignment for Young Neutron Stars. *ApJ*, 677:1201-1215, Apr. 2008. doi: 10.1086/529026.
- V. Khaire and R. Srianand. New synthesis models of consistent extragalactic background light over cosmic time. *MNRAS*, 484(3):4174–4199, Apr. 2019. doi: 10.1093/mnras/stz174.
- T. Kifune. Invariance Violation Extends the Cosmic-Ray Horizon? *ApJL*, 518:L21–L24, June 1999. doi: 10.1086/312057.
- F. Kislat and H. Krawczynski. Search for anisotropic Lorentz invariance violation with γ -rays. *Phys. Rev. D*, 92:045016, Aug 2015. doi: 10.1103/PhysRevD.92.045016.
- S. Koushan et al. GAMA/DEVILS: constraining the cosmic star formation history from improved measurements of the 0.3-2.2 μm extragalactic background light. *MNRAS*, 503(2):2033–2052, May 2021. doi: 10.1093/mnras/stab540.
- R. G. Lang, H. Martínez-Huerta, and V. de Souza. Improved limits on Lorentz invariance violation from astrophysical gamma-ray sources. *Phys. Rev. D*, 99:043015, Feb 2019. doi: 10.1103/PhysRevD.99.043015. URL <https://link.aps.org/doi/10.1103/PhysRevD.99.043015>.

- L. R. Levenson and E. L. Wright. Probing the 3.6 μm CIRB with Spitzer in Three DIRBE Dark Spots. *ApJ*, 683:585-596, Aug. 2008. doi: 10.1086/589808.
- C. Lunardini. Diffuse supernova neutrinos at underground laboratories. *Astroparticle Physics*, 79: 49–77, June 2016. doi: 10.1016/j.astropartphys.2016.02.005.
- P. Madau and L. Pozzetti. Deep galaxy counts, extragalactic background light and the stellar baryon budget. *MNRAS*, 312:L9–L15, Feb. 2000. doi: 10.1046/j.1365-8711.2000.03268.x.
- MAGIC Collaboration, V. A. Acciari, et al. Measurement of the extragalactic background light using MAGIC and Fermi-LAT gamma-ray observations of blazars up to $z = 1$. *MNRAS*, 486(3): 4233–4251, July 2019a. doi: 10.1093/mnras/stz943.
- MAGIC Collaboration, V. A. Acciari, et al. Teraelectronvolt emission from the γ -ray burst GRB 190114C. *Nature*, 575(7783):455–458, Nov 2019b. doi: 10.1038/s41586-019-1750-x.
- MAGIC Collaboration, V. A. Acciari, L. Nava, et al. Bounds on Lorentz Invariance Violation from MAGIC Observation of GRB 190114C. *Phys. Rev. Lett.*, 125:021301, Jul 2020. doi: 10.1103/PhysRevLett.125.021301. URL <https://link.aps.org/doi/10.1103/PhysRevLett.125.021301>.
- M. Martínez and M. Errando. A new approach to study energy-dependent arrival delays on photons from astrophysical sources. *Astrop. Phys.*, 31:226–232, Apr. 2009. doi: 10.1016/j.astropartphys.2009.01.005.
- H. Martínez-Huerta, R. G. Lang, and V. de Souza. Lorentz invariance violation tests in astroparticle physics. *Symmetry*, 12(8), 2020. ISSN 2073-8994. doi: 10.3390/sym12081232. URL <https://www.mdpi.com/2073-8994/12/8/1232>.
- S. Matsuura et al. New Spectral Evidence of an Unaccounted Component of the Near-infrared Extragalactic Background Light from the CIBER. *ApJ*, 839:7, Apr. 2017. doi: 10.3847/1538-4357/aa6843.
- K. Mattila and P. Väisänen. Extragalactic background light: inventory of light throughout the cosmic history. *Contemporary Physics*, 60(1):23–44, Jan. 2019. doi: 10.1080/00107514.2019.1586130.
- K. Mattila et al. Extragalactic background light: a measurement at 400 nm using dark cloud shadow*- I. Low surface brightness spectrophotometry in the area of Lynds 1642. *MNRAS*, 470: 2133–2151, Sept. 2017a. doi: 10.1093/mnras/stx1295.
- K. Mattila et al. Extragalactic background light: a measurement at 400 nm using dark cloud shadow - II. Spectroscopic separation of the dark cloud’s light, and results. *MNRAS*, 470:2152–2169, Sept. 2017b. doi: 10.1093/mnras/stx1296.
- A. Neronov and D. V. Semikoz. A method of measurement of extragalactic magnetic fields by TeV gamma ray telescopes. *JETP Letters*, 85(10):473–477, Jul 2007. ISSN 1090-6487. doi: 10.1134/S0021364007100013.

- A. Neronov and D. V. Semikoz. Sensitivity of γ -ray telescopes for detection of magnetic fields in the intergalactic medium. *Phys. Rev. D*, 80(12):123012, Dec. 2009. doi: 10.1103/PhysRevD.80.123012.
- A. I. Nikishov. Absorption of High-Energy Photons in the Universe. *Soviet Physics JETP*, 14(2): 393–394, Feb. 1962.
- M. R. Orr, F. Krennrich, and E. Dwek. Strong New Constraints on the Extragalactic Background Light in the Near- to Mid-infrared. *ApJ*, 733:77, June 2011. doi: 10.1088/0004-637X/733/2/77.
- I. Rafighi, S. Vafin, M. Pohl, and J. Niemiec. Plasma effects on relativistic pair beams from TeV blazars: PIC simulations and analytical predictions. *A&A*, 607:A112, Nov. 2017. doi: 10.1051/0004-6361/201731127.
- A. Reimer. The Redshift Dependence of Gamma-Ray Absorption in the Environments of Strong-Line AGNs. *ApJ*, 665:1023–1029, Aug. 2007. doi: 10.1086/519766.
- A. G. Riess et al. New Parallaxes of Galactic Cepheids from Spatially Scanning the Hubble Space Telescope: Implications for the Hubble Constant. *ApJ*, 855:136, Mar. 2018. doi: 10.3847/1538-4357/aaadb7.
- C. Rovelli. Loop Quantum Gravity. *Living Reviews in Relativity*, 11:5, Jul 2008. doi: 10.12942/lrr-2008-5.
- M. H. Salamon, F. W. Stecker, and O. C. de Jager. A new method for determining the Hubble constant from sub-TeV gamma-ray observations. *ApJL*, 423:L1–L4, Mar. 1994. doi: 10.1086/187221.
- A. Saldana-Lopez et al. An observational determination of the evolving extragalactic background light from the multiwavelength HST/CANDELS survey in the Fermi and CTA era. *MNRAS*, 507(4):5144–5160, Nov. 2021. doi: 10.1093/mnras/stab2393.
- D. A. Sanchez, S. Fegan, and B. Giebels. Evidence for a cosmological effect in γ -ray spectra of BL Lacertae. *A&A*, 554:A75, June 2013. doi: 10.1051/0004-6361/201220631.
- L. Sironi and D. Giannios. Relativistic Pair Beams from TeV Blazars: A Source of Reprocessed GeV Emission rather than Intergalactic Heating. *ApJ*, 787:49, May 2014. doi: 10.1088/0004-637X/787/1/49.
- F. Tavecchio and G. Bonnoli. On the detectability of Lorentz invariance violation through anomalies in the multi-TeV γ -ray spectra of blazars. *A&A*, 585:A25, Jan. 2016. doi: 10.1051/0004-6361/201526071.
- A. M. Taylor, I. Vovk, and A. Neronov. Extragalactic magnetic fields constraints from simultaneous GeV-TeV observations of blazars. *A&A*, 529:A144, May 2011. doi: 10.1051/0004-6361/201116441.
- T. Vachaspati. Progress on Cosmological Magnetic Fields. *Reports on Progress in Physics*, 84(7), 6 2021. doi: 10.1088/1361-6633/ac03a9.

- S. Vafin, I. Rafighi, M. Pohl, and J. Niemiec. The Electrostatic Instability for Realistic Pair Distributions in Blazar/EBL Cascades. *ApJ*, 857:43, Apr. 2018. doi: 10.3847/1538-4357/aab552.
- V. Vasileiou et al. Constraints on Lorentz invariance violation from Fermi-Large Area Telescope observations of gamma-ray bursts. *Phys. Rev. D*, 87:122001, Jun 2013. doi: 10.1103/PhysRevD.87.122001. URL <https://link.aps.org/doi/10.1103/PhysRevD.87.122001>.
- F. Vazza et al. Simulations of extragalactic magnetic fields and of their observables. *Classical and Quantum Gravity*, 34(23):234001, Dec. 2017. doi: 10.1088/1361-6382/aa8e60.
- VERITAS Collaboration, A. U. Abeysekara, et al. Measurement of the Extragalactic Background Light Spectral Energy Distribution with VERITAS. *ApJ*, 885(2):150, Nov. 2019. doi: 10.3847/1538-4357/ab4817.
- P. S. Wesson. Olbers's paradox and the spectral intensity of the extragalactic background light. *ApJ*, 367:399–406, Feb. 1991. doi: 10.1086/169638.
- M. Zemcov, P. Immel, C. Nguyen, A. Cooray, C. M. Lisse, and A. R. Poppe. Measurement of the cosmic optical background using the long range reconnaissance imager on New Horizons. *Nature Communications*, 8:15003, Apr. 2017. doi: 10.1038/ncomms15003.